water

MDPI

Review

Remote Sensing Technology in the Construction of Digital Twin Basins: Applications and Prospects

Xiaotao Wu [1,2,*], Guihua Lu [2] and Zhiyong Wu [2]

[1] Shanghai Investigation Design Research Institute, Shanghai 200335, China
[2] College of Hydrology and Water Resources, Hohai University, Nanjing 210098, China; lugh@hhu.edu.cn (G.L.); wuzhiyong_110@163.com (Z.W.)
* Correspondence: zjyelaoma@126.com

Abstract: A digital twin basin serves as a virtual representation of a physical basin, enabling synchronous simulation, virtual–real interaction, and iterative optimization. The construction of a digital twin basin requires a basin database characterized by large-scale coverage, high-precision, high-resolution, and low-latency attributes. The advancements in remote sensing technology present a new technical means for acquiring essential variables of the basin. The purpose of this paper was to provide a comprehensive overview and discussion of the retrieval principle, data status, evaluation and inter-comparison, advantages and challenges, applications, and prospects of remote sensing technology in capturing seven essential variables, i.e., precipitation, surface temperature, evapotranspiration, water level, river discharge, soil moisture, and vegetation. It is indicated that remote sensing can be applied in some digital twin basin functions, such as drought monitoring, precipitation forecasting, and water resources management. However, more effort should be paid to improve the data accuracy, spatiotemporal resolution, and latency through data merging, data assimilation, bias correction, machine learning algorithms, and multi-sensor joint retrieval. This paper will assist in advancing the application of remote sensing technology in constructing a digital twin basin.

Keywords: digital twin basin; satellite remote sensing; unmanned aerial vehicle; meteorology; hydrology

Citation: Wu, X.; Lu, G.; Wu, Z. Remote Sensing Technology in the Construction of Digital Twin Basins: Applications and Prospects. *Water* **2023**, *15*, 2040. https://doi.org/10.3390/w15112040

Academic Editors: Kairong Lin, Jingwen Zhang and Pan Yang

Received: 19 April 2023
Revised: 19 May 2023
Accepted: 22 May 2023
Published: 27 May 2023

1. Introduction

The concept of a digital twin has garnered substantial attention in recent years due to its efficacy as a potent tool for simulating and managing complex real-world systems [1]. A digital twin is a virtual representation of a physical product, system, or process that facilitates real-time monitoring, simulation, analysis, and management [2,3]. In the field of hydrology and water resources, a digital twin basin serves as a virtual representation of a physical basin, enabling synchronous simulation, virtual–real interaction, and iterative optimization [4]. Essentially, a digital twin basin facilitates a comprehensive understanding of the water and energy cycles within a basin, while also providing vital decision support for government agencies [5,6].

The construction of a digital twin basin requires a basin database characterized by large-scale coverage, high-precision, high-resolution, and low-latency attributes [7,8]. Such a database can be obtained through two primary methods: in situ measurements and remote sensing [8]. In situ measurements involve the direct observation of the basin's parameters and variables through ground-based monitoring stations. This approach provides precise and accurate data at the local scale, enabling detailed analysis and understanding of specific points within the basin. However, in situ measurements have limitations in terms of low spatial coverage and they are labor-intensive, which hinders the ability to capture basin-wide dynamics and may result in data gaps in remote or inaccessible regions [9]. On the other hand, remote sensing has emerged as a recent advancement in basin observation [10].

Remote sensing refers to a technology that employs non-contact detection techniques to extract, process, analyze, and apply electromagnetic wave information that is reflected, radiated, or scattered by distant objects [11–13]. By utilizing satellite or airborne sensors, remote sensing enables large-scale, synchronized, and timely data acquisition, providing a comprehensive data view of the basin.

In recent years, advancements in sensor technology and retrieval algorithms have significantly improved data quality and accessibility of remote sensing observations [13,14]. These advancements have facilitated the utilization of remote sensing data in various water conservancy applications, such as basin flood forecasting, drought monitoring, water resources evaluation, and soil and water conservation analysis [15]. In ungauged basins, remote sensing serves as a valuable source of data for hydrological simulation and prediction. For instance, Du [16] utilized satellite-retrieved glacier, precipitation, temperature, and water level data to simulate a runoff time series in the Tibetan Plateau. In addition, remote sensing-based observations can extend the scale of disaster monitoring, such as drought from the local scale to a larger regional scale. For instance, Zhang et al. [17] developed a drought index based on satellite-retrieved precipitation, soil moisture, and surface temperature data, establishing a satellite-based drought monitoring system in northern China.

Although remote sensing provides a promising data source for the construction of digital twin basins, several challenges still need to be addressed. Firstly, the long re-visit periods of satellites results in inadequate temporal resolution, restricting the availability of observational data and the ability to track rapid changes in observed variables [18]. Consequently, applying such remote sensing data to hour-scale flood forecast applications in digital twin basins becomes challenging. To address this challenge, some researchers have developed a data assimilation framework that integrates land surface models and remote sensing observations to fill in the temporal gaps and enhance temporal resolution. For instance, Chao et al. [19] developed a framework for assimilation of satellite-based soil moisture data into the WRF-Hydro model based on the EnKF algorithm for flood forecasting. Secondly, certain sensors, such as the microwave radiometer, suffer from insufficient spatial resolution due to their long wavelengths [20]. Consequently, the application of such remote sensing data to small basins poses challenges. So far, many scholars have conducted research on downscaling methodologies to enhance the spatial resolution of remote sensing observations. For instance, Liu et al. [21] proposed an attention mechanism-based convolution network to downscale satellite-based precipitation data from a coarser spatial resolution of 0.1° to a finer resolution of 0.01°. Thirdly, the time series of individual remote sensing products is usually not long enough for hydrological applications. One promising solution to this issue is the merging of multi-source remote sensing products [22]. For example, Dorigo et al. [23] developed a data merging framework employing a triple collocation algorithm, incorporating data from 12 remote sensing soil moisture products to generate a satellite-based soil moisture product spanning the period from 1978 to 2022.

The recent advancements in remote sensing technology have made it a valuable tool and data source with both promise and challenges. However, there is currently a lack of review papers in the literature that comprehensively investigate and discuss the applications and prospects of remote sensing technology in the construction of digital twin basins. In view of this, the goal of this paper was to provide a comprehensive overview of the retrieval principles, data status, existing challenges, and future prospects of remote sensing technology in capturing seven essential variables, i.e., precipitation, surface temperature, evapotranspiration, water level, river discharge, soil moisture, and vegetation. Section 2 provides a concise overview of the classification, characteristics, and applications of the electromagnetic spectrum in remote sensing. Section 3 focuses on the applications and prospects of seven remote sensing variables in digital twin basins. For each variable, the retrieval principle, data status, evaluation and inter-comparison, advantages and challenges, applications, and future outlooks are reviewed and discussed

in order. The conclusion of this paper will assist in advancing the application of remote sensing technology in constructing a digital twin basin.

2. Overview of Remote Sensing Technology

This section provides an overview of remote sensing technology, which refers to the non-contact detection technology that processes and analyzes reflected, radiated, or scattered electromagnetic waves from objects [24]. Electromagnetic waves are categorized according to the wavelength range, including ultraviolet (10 to 400 nm), visible spectral (400 to 700 nm), infrared (700 nm to 1 mm), microwave (1 mm to 1 m), and longer wavelengths. Among these, visible spectral, near-infrared, thermal infrared, and microwave remote sensing are the most commonly used in remote sensing applications [25]. Visible spectral and near-infrared remote sensing in the visible light and infrared bands are collectively referred to as visible spectral remote sensing, as they receive electromagnetic waves from the surface reflection of sunlight. This range provides ultra-high resolution and full-color images. However, it is significantly constrained by sunlight and cloud conditions [26,27]. On the other hand, in the thermal infrared and microwave bands, with wavelengths exceeding 3 μm, there are fewer limitations posed by cloud cover and sunlight. Thermal infrared remote sensing enables the establishment and training of retrieval models between thermal infrared information and object temperature. Hence, it finds wide applications in wildfire monitoring, surface temperature retrieval, and other relevant research [28]. Figure 1 shows the electromagnetic spectrum classification and its corresponding applications.

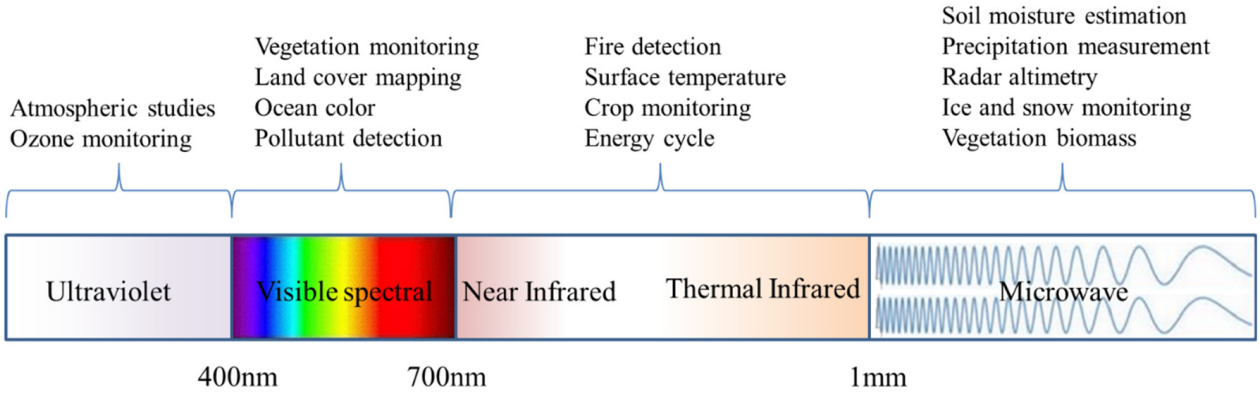

Figure 1. Electromagnetic spectrum classification and its corresponding applications.

Microwave remote sensing employs longer wavelength microwave bands than both visible spectral remote sensing and thermal infrared remote sensing, which makes it capable of penetrating through clouds, vegetation, and surfaces more efficiently. Consequently, meteorological, cloud, and sunshine conditions have minimal impact on microwave remote sensing, making it an excellent tool for all-day and all-weather continuous operations. Despite this advantage, the spatial resolution of microwave remote sensing tends to be coarser due to its longer wavelength [29]. The bands used in microwave remote sensing are categorized as K, Ku, X, G, C, S, Ls, and L according to their frequencies. Among these bands, the X, C, and L bands are the most widely used in soil moisture and ocean observations, while the K band is widely used for cloud and water vapor observations. In terms of sensor technology, microwave remote sensing can be divided into active and passive microwave remote sensing [20]. Active microwave remote sensing refers to the use of a microwave transmitter such as synthetic aperture radar (SAR) to illuminate an area of interest and then receiving the reflected microwaves from that area using a receiver. Passive microwave remote sensing, on the other hand, refers to the detection of naturally occurring microwave radiation emitted by the Earth's surface and atmosphere by microwave radiometers [30]. Active microwave remote sensing typically has higher spatial resolution than passive remote sensing due to the different working principles of

the sensors. However, the accuracy of active microwave remote sensing is more likely to be affected by environmental factors such as water bodies. Joint retrieval is the process of combining data from both active and passive microwave sensors to improve the accuracy and resolution of the measurements, which is the main direction of research in the retrieval of future earth variables [31,32].

3. Applications and Prospects of Remote Sensing in Digital Twin Basin Construction

3.1. Precipitation

Precipitation plays a crucial role in global water and energy cycles as it drives hydrological processes [32,33]. Accurate, high-resolution, real-time precipitation data are crucial for effective flood forecasting, drought monitoring, and water resource management, all of which are primary objectives of digital twin basin functionality [34–36].

Currently, precipitation can be measured using two methods: ground-based observations by rain gauge stations and remote sensing-based observations by sensors [37]. Remote sensing-based retrieval can further be categorized into ground-based radar observations and satellite remote sensing-based retrieval. Ground-based observations by rain gauge stations are the most accurate means of obtaining precipitation data and have been established for a long time with long sequences of data. However, due to factors such as labor costs, economic viability, terrain complexity, and other considerations, achieving large-scale and high-resolution precipitation observations is difficult [38]. Ground-based radar observations, which employ the active emission of electromagnetic waves and analysis of signals scattered by raindrops, can obtain high-precision and high-resolution precipitation data on a regional scale. However, this method still has several limitations, including short time series, high cost, and high terrain requirements [39]. Presently, there are over 200 ground-based radars in China that are mainly concentrated in the southeast coastal areas and sparsely located in the northwest region. Satellite remote sensing, on the other hand, retrieves precipitation data by receiving cloud-reflected signals through satellite-borne sensors, allowing large-scale and all-day precipitation observations, particularly in ungauged basins such as in Western China. However, the uncertainty and spatiotemporal resolution of satellite remote sensing-based precipitation data remain crucial challenges to be solved [40]. The most commonly used satellite remote sensing-based precipitation datasets include TRMM (Tropical Rainfall Measuring Mission), GPM (Global Precipitation Measurement), GSMaP (Global Satellite Mapping of Precipitation), and China's Fengyun-2 series satellite precipitation data. Table 1 summarizes these mainstream satellite-based precipitation products with the corresponding data acquisition methods, spatiotemporal resolution, and coverage. Over the years, significant improvements have been made in data acquisition methods and spatiotemporal resolution. Additionally, this table shows the transitioning from traditional single-satellite-based retrieval to multi-sensor or multi-satellite-based joint retrieval, such as the GPM series precipitation satellites. Figure 2 illustrates the composition of the GPM series precipitation satellites.

Researchers have employed different validation and evaluation methods to assess the precision and uncertainty of satellite-based precipitation products across diverse regions [41]. This study reviewed previous research related to the evaluation and intercomparison of these data products, aiming to enhance our understanding of their quality and associated challenges within various areas. Table 2 presents a summary of author names, data sources, study areas, and major conclusions from the corresponding reviewed studies. In general, satellite-based precipitation products are becoming a reliable data source with acceptable accuracy in various river basins around the world, especially in ungauged regions such as the Tibetan Plateau. On the other hand, calibration and validation before data application are still indispensable in order to avoid uncertainty.

Table 1. Summary of typical satellite precipitation products.

Product	Method	Spatial Resolution	Temporal Resolution	Spatial Coverage	Temporal Coverage
GPCP	Infrared and microwave sensors	2.5°	1 month	60° N~60° S	1979~present
CMAP	Satellite and ground data merging	2.5°	5 d	60° N~60° S	1979~present
TRMM	Precipitation radar PR, microwave TMI	0.25°	3 h	50° N~50° S	1997~2015
PERSIANN	ANN based merging using multi-satellite	0.25°	1 d	60° N~60° S	1982~present
CMORPH	MPRPH deformation algorithm for microwave sensor and infrared sensor data	0.25°	30 min	60° N~60° S	1998~present
GPM	Series satellites: equipped with Ku/Ka dual-frequency precipitation radar and multichannel microwave imager	0.1°	30 min	Global	2014~present
GSMaP	GPM satellite retrieval by JAXA	0.1°	30 min	Global	2014~present
IMERG	NASA integrated satellite inversion based on TRMM and GPM	0.1°	30 min	Global	2000~present

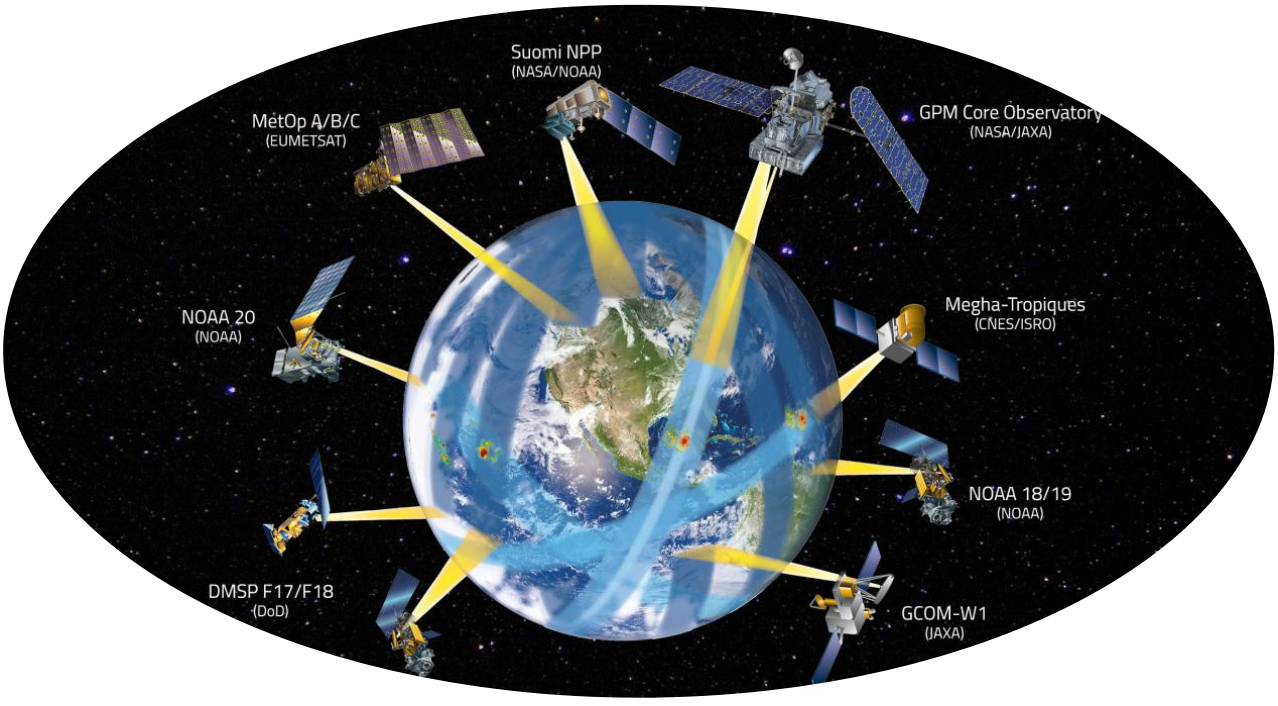

Figure 2. Composition of the GPM series precipitation satellites https://gpm.nasa.gov/ (accessed on 6 April 2023).

Table 2. Evaluation and inter-comparison of different satellite-based precipitation products over different regions.

Study	Data	Area	Conclusions
[42] (2020)	GSMaP	China	The calibration of GSMaP_NRT using a gauge-adjusted, near-real-time GSMaP precipitation estimate (GSMaP_Gauge_NRT) effectively reduced this bias and was more consistent with gauge observations. The correction scheme mainly acted on hit events and could hardly make up the missed events of the satellite-based precipitation estimates. The correction results were in good agreement with the original GSMaP data globally.
[43] (2020)	CMORPH/ IMERG	United Arab Emirates	IMERG was significantly better than CMORPH in detecting rainfall observed by the gauge network. Both products performed quite well in rainfall detection, but reported rainfall was not observed by the rain gauges at an alarming rate, especially for light rain, while for moderate and intense (upper quartiles) rainfall rates, performance was much better.
[44] (2021)	IMERG/ TRMM	United States	IMERG and its predecessor TRMM 3B42 performed better in the eastern CONUS than in the mountainous western CONUS. The evaluation demonstrated the clear improvement in the IMERG precipitation product, especially in reducing missed precipitation in winter and summer and hit bias in winter, resulting in better performance in capturing lighter and heavier precipitation.
[45] (2022)	PERSIANN/ GPCP	Sudan	Satellite-based precipitation datasets had significant uncertainties, and the quantile mapping (QM) method could be applied to correct the systematic bias.
[46] (2022)	PERSIANN/ GPCP	Pakistan	The performance of the precipitation products was improved by increasing the temporal and spatial scales. The feasibility of certain precipitation products for streamflow prediction in other semi-arid regions of the world should be further studied. Combinations of different hydrological models should be used along with a suite of precipitation products that have different development mechanisms.
[47] (2022)	TRMM/ PERSIANN/ CMAP/ GPCP/ CMORPH	East Africa	All products showed systematic errors in rainfall retrieval that decreased with an increase in rainfall amount (>100 mm/month). CMORPH and TRMM showed consistently high performance during March to May (MAM) and October to December (OND) rainy seasons. The effect of elevation variation was more evident during the OND season.
[48] (2022)	TRMM/ PERSIANN/ CMORPH	Tibetan Plateau	All products overestimated the precipitation at 0.1–5 mm/d and underestimated the precipitation above 5 mm/d, especially for PERSIANN. TRMM showed relatively stable performance for various elevations and climate zones. For hydrological model validation, TRMM had the best performance during the calibration period. Overall, TRMM had the highest applicability in the study area, however, its impact on the uncertainty of hydrological modeling needs to be further studied.
[49] (2022)	PERSIANN	California, USA	PERSIANN-Cloud Classification System–Climate Data Record (CCS–CDR) had the least bias among all PERSIANN family datasets, while the two near-real-time datasets, PERSIANN–Dynamic Infrared Rain Rate (PDIR), performed significantly more accurately than PERSIANN-Cloud Classification System (CCS). In simulating streamflow, CSS-CDR and PDIR also had accurate estimations.

Table 2. *Cont.*

Study	Data	Area	Conclusions
[50] (2022)	PERSIANN	Contiguous United States	The extreme gradient boosting (XGBoost) and random forest algorithms were the most accurate in terms of the squared error scoring function. The remaining algorithms could be ordered as follows, from best to tworst: Bayesian regularized feed-forward neural networks, poly-MARS, gbm, MARS, feed-forward neural networks, and linear regression.
[51] (2023)	GPCP/ PERSIANN/ CMORPH/ GPM/ GSMaP	Xiangjiang Basin, China	GSMaP ranked as the best-performing satellite precipitation product with the overall statistical metrics, while GSMaP gave the closest agreement with the observations. Additionally, the GSMaP-driven model was also superior in depicting the rainfall–runoff relationship. However, satellite remote sensing still had difficulty accurately estimating precipitation over a mountainous region.
[52] (2023)	IMERG/ TRMM/ PERSIANN	Central Asia	The performance of all products was more capable on a monthly scale than on a daily scale. All products showed underestimations in the summer season. They showed better performance in capturing light precipitation events while IMERG performed best in daily, monthly, and seasonal estimations and was capable of being used in hydro-climatic applications over the mountainous domain of Central Asia. The performance of PERSIANN-CDR and TRMM was acceptable at low topography.
[53] (2023)	GSMaP/ IMERG	Tibetan Plateau	The correction of precipitation measurements with the machine learning method (XGBoost regression) outperformed the traditional statistical method in accuracy metrics and frequency distribution, offering a promising strategy for obtaining more accurate precipitation measurements in high-altitude regions.
[54] (2023)	PERSIANN/ IMERG	Contiguous United States	Tree-based ensemble algorithms are adopted in various fields for solving regression problems with high accuracy and low computational costs. The results indicated that extreme gradient boosting (XGBoost) was more accurate than random forest and gradient boosting machine (gbm), and IMERG was more useful than PERSIANN.

The construction of a digital twin basin necessitates high-precision, high-resolution, and low-latency precipitation data. To improve the data accuracy, satellite-based precipitation data need preprocessing, bias correction, or calibration to match the requirements of digital twin basins. To date, the most promising approach for obtaining top-quality precipitation data is through multi-source data merging [55,56]. The categories of data merging algorithms include bias correction, interpolation distribution, multivariate regression, and machine learning [57]. Tang [58] validated and evaluated the accuracy of GPM satellite-based precipitation data globally, and proposed a deep learning algorithm that merged passive microwave, infrared, and environmental data to enhance the data quality. Liu [21] developed a multi-source data merging model for precipitation using the random forest method and relied on radar precipitation and remote sensing precipitation data in southwestern China. In terms of spatiotemporal resolution improvement, statistical downscaling, dynamic downscaling, hybrid downscaling, optimal interpolation, and other methods can be used. Sun et al. [59] employed an optimal interpolation algorithm to create a high-resolution precipitation dataset for nearly 20 years based on ground-based precipitation data and TRMM remote sensing-based precipitation data in Jiangsu Province. For monitoring urban extreme precipitation, the latest technology permits the acquisition of a 100-m grid and 1-min interval precipitation map using microwave link-based monitoring; this technology is based on communication base stations [60]. Jiangyin City has imple-

mented this technology to set up a network for monitoring in key urban areas, which has significantly enhanced precipitation monitoring accuracy [61]. In addition, satellite-based precipitation data should be available in real-time or near real-time to provide up-to-date information for the requirements of digital twin basins. Delays in data processing, quality control, and dissemination can affect the usefulness of satellite-based precipitation data for digital twin basin applications such as flood forecasting.

In conclusion, the application of satellite-based precipitation data provides significant potential for digital twin basin construction. However, there are still several challenges, such as accuracy, resolution, and latency, that need to be assessed. Future research should focus more on multi-source data merging, calibration and bias correction, high-resolution retrieval algorithms, and modified downscaling algorithms. Additionally, attention must be paid to computer hardware capabilities, such as parallel computing or GPU-accelerated computing, which can help reduce the processing latency of satellite data.

3.2. Surface Temperature

Surface temperature is a critical variable for land surface biological and physical processes, including vegetation photosynthesis, evaporation, and wildfire monitoring [62]. It is also a key driving factor for water and energy cycles and holds significant research significance in fields such as agriculture, ecology, hydrology, meteorology, and others [63]. Reliable surface temperature data are essential for hydrological modeling in digital twin basins.

Ground-based meteorological stations serve as the primary method for surface temperature observation, offering extensive time series data and high levels of accuracy. Surface temperature data in areas lacking meteorological stations are obtained through interpolation from nearby stations, leading to decreased accuracy in sparsely networked regions [64,65]. Compared with ground-based temperature measurements, the advantages of satellite-based surface temperature data include wide coverage, data consistency, cost-effectiveness, and data accessibility. Since the 1980s, temperature retrieval algorithms have been developed based on several earth-synchronous and polar orbit, sun-synchronous satellites [64]. The temporal resolution of earth-synchronous satellite-based temperature data is generally around 15 min, with a spatial resolution typically exceeding 5 km. On the other hand, the spatial resolution of polar orbit, sun-synchronous satellite-based temperature data is typically below 60 m, while the temporal resolution is usually greater than 2 days. Currently, the primary methods for temperature retrieval include the atmospheric profile extrapolation method, energy balance method, statistics method, temperature-vegetation index method, and machine learning method [66]. Table 3 presents the details of mainstream remote sensing temperature products, including the satellite carrier, sensor model, spatiotemporal resolution, and time series. The table indicates that with advancements in sensor technology, the spatial resolution of remote sensing temperature products has progressed from an initial 1 km to 30 m, while the temporal resolution has improved from 16 days to 10 min.

Many studies have been conducted to validate the precision and uncertainty of satellite-based surface temperature products across diverse regions. We reviewed previous research related to the evaluation of these data products to enhance the understanding of data quality and challenges. Table 4 presents a summary of author names, data sources, study areas, and major conclusions from the corresponding reviewed studies. In general, the accuracy of satellite-based surface temperature products varies a lot in different regions due to the various land cover types, topography, heterogeneity, surface roughness, vegetation, and climate [67]. For example, data retrieval in regions with dense vegetation cover suffers more uncertainty compared to that in regions with bare soil or urban areas. In addition, although land surface temperature retrieval based on Modis and Landsat is still the most commonly used, the emergence of new satellites, such as Sentinel series and Fengyun series satellites, will bring prospects for more accurate and higher resolution land surface temperature retrieval in the future.

Table 3. Summary of typical satellites for surface temperature retrieval.

Satellite	Sensor	Spatial Resolution	Temporal Resolution	Temporal Coverage
Terra/Aqua	Moderate Resolution Imaging Spectroradiometer (MODIS)	1 km	1 d	1999~present
Landsat5	Thematic Cartograph TM	60 m	16 d	1984~2012
Landsat7	Enhanced thematic mapper ETM+	30 m	16 d	1999~2022
Landsat8	Land Imager OLI	30 m	16 d	2013~present
Landsat9	Land imager OLI-2	15 m	16 d	2022~present
GOES-16	Advanced Baseline Imager ABI	1 km	15 min	2016~present
Himawari-8	Multichannel visible infrared radiometer	500 m	10 min	2015~present
FY-4A	Multichannel scanning imager	500 m	15 min	2018~present
Sentinel-3	Sea and Land Surface Temperature Radiometer	500 m	1 d	2016~present

Table 4. Evaluation of different satellite-based surface temperature products over different regions.

Study	Data	Area	Conclusions
[68] (2017)	MODIS	Northeast China	Surface temperature could be accurately estimated using remote sensing, but the model performance was varied across different spatial and temporal scales.
[69] (2018)	Himawari-8	East Asia	The accuracy of the algorithm was slightly dependent on the season and time of day, showing better performance during the warm season at night. Additionally, the accuracy of the algorithm decreased when the lapse rate exceeded 10 K and brightness temperature difference exceeded 6 K.
[70] (2020)	Landsat8	Conterminous United States	The uncertainty in downwelling and upwelling radiance had a similar effect on LST in both daytime and nighttime, but uncertainty from broadband emissivity was half as much at night. Overall, all LST retrieval methods applied to nighttime data provided highly accurate results with different LSE models and lower bias compared to in situ measurements.
[71] (2021)	MODIS	Global	Climate Forecast System Version 2 (CFSv2)-modeled temperatures were combined with MODIS LST to derive a continuous gap-filled global LST dataset at a spatial resolution of 1 km. The gap-filled LST dataset had high accuracy and could be used for various applications that require continuous LST data. The accuracy was evaluated in nine regions across the globe using cloud-free LST (mean values: R^2 = 0.93, RMSE = 2.7 °C).
[72] (2021)	Landsat5/ Landsat7/ Landsat8	Conterminous United States	The Landsat LST product had a relatively consistent performance among Landsat 5, 7, and 8 sensors and could be used for various applications over snow-free land surfaces, snow-covered surfaces, and water surfaces.
[73] (2021)	Landsat8/ MODIS	Gansu, China	The fusion algorithm produced good results, and ESTARFM had the highest fusion accuracy compared to STARFM and FSDAF. The Landsat 8 LST product was highly consistent with ground measurements, and the fusion images were highly consistent with actual Landsat 8 LST images, indicating the reliability of the fusion results.

Table 4. *Cont.*

Study	Data	Area	Conclusions
[74] (2021)	Sentinel-3	Valencia, Spain	The study proposed emissivity-dependent split-window algorithms with angular dependence for the Sentinel-3 SLSTR sensor. It was found to provide more accurate and precise LSTs than the current version of the operational SLSTR product.
[75] (2022)	MODIS	Global	The data interpolating empirical orthogonal functions and the CDF-based correction method could effectively reconstruct missing LST data and guarantee acceptable accuracy (with RMSEs of 1–2 K and R values of 0.820–0.996) in most regions of the world at 0.05° pixel grid.
[76] (2022)	MODIS	Heihe Basin, China	The scheme proposed in this study was able to accurately reconstruct missing values and improve the accuracy of the interpolation method to a certain extent when reconstructing MODIS land surface temperature.
[77] (2022)	Sentinel-3	Košice, Slovakia	A multiple linear regression model based on spectral indices and LST from Landsat 8 data could be used to predict LST at 10 m resolution using Sentinel-2 data, resulting in a better perception of the LST field associated with land cover features present in the urban environment, aiding in urban decision-making and planning to improve citizens' quality of life.
[78] (2023)	FY-4A	China	Overall, the preferred algorithm exhibited good accuracy and met the required accuracy of the FY-4A mission. However, the validation showed that the FY-4A LST official product accuracy was low in seasons with large atmospheric water vapor.

Although satellite-based surface temperature data have been used in many studies, several challenges need to be solved, including atmospheric interference, cloud cover, and data gaps [79]. On the other hand, higher temporal and spatial resolutions are necessary to fulfill the needs of digital twin basin requirements. Therefore, many scholars have developed relevant algorithms to improve the spatiotemporal resolution of land surface temperature. For example, Chen et al. [80] presented a dictionary merging algorithm based on polar orbit, sun-synchronous satellite Fengyun-3 and earth-synchronous satellite Fengyun-4 data to acquire Hunan Province's temperature data with a 1 h temporal resolution and a 250 m spatial resolution. However, the uncertainty caused by atmospheric radiation in specific regions may affect the quality of satellite-based temperature products; therefore, some scholars have conducted temperature merging experiments involving ground observations and remote sensing temperatures for better results. For instance, Zhou et al. [81] improved the effectiveness of temperature retrieval by utilizing the HASM-GWR merging algorithm based on 190 station-based temperature series and MODIS remote sensing temperature data.

While satellite-based surface temperature products offer great utility for digital twin basins with advances in sensors and algorithms, mitigating the challenges such as atmospheric and cloud interference remains crucial to generating suitable data with good quality. Future research should focus more on calibration and validation, multi-sensor joint retrieval, and new algorithm development such as reinforcement learning.

3.3. Evapotranspiration

Evapotranspiration refers to the combined process of evaporation and transpiration that occurs in the basin water cycle, which encompasses soil evaporation, vegetation transpiration, canopy interception evaporation, and water surface evaporation [82]. Evapotranspiration serves as a fundamental link between the atmosphere, hydrosphere, and biosphere, and constitutes a core variable in the balance of water and energy in the earth's land surface [83]. Over half of global precipitation and solar energy enter the earth's water and energy cycles via evapotranspiration, making it crucial to many research fields including hydrology, water resources, agricultural irrigation, and drought monitoring [84,85]. Accurate evapotranspiration data have important decision-making significance for the functions of digital twin basins, such as drought monitoring and water resource management.

Evapotranspiration can be obtained using instruments such as lysimeters and large-aperture scintillometers [86]. However, the spatial representativeness of local evapotranspiration is inadequate due to the presence of complex underlying surfaces [87]. Consequently, researchers have proposed both empirical and physical methods to calculate evapotranspiration. The Penman–Monteith equation is the most widely employed method for its consideration of energy balance and water vapor diffusion principles. It provides a simple and accurate calculation, relying solely on meteorological data such as temperature, water vapor pressure, and wind speed. However, its accuracy is influenced by both meteorological data and the presence of complex underlying surfaces [88,89]. Advances in remote sensing technology have made it possible to acquire large-scale and high-precision meteorological and underlying surface data. Using the Penman–Monteith equation and high-quality underlying data, researchers have established the relationship between vegetation indices, soil, vegetation, and near-surface atmospheric impedance parameters through machine learning and data assimilation. This enables further calculation of evapotranspiration data, exemplified by products such as MOD16, PLSH, and MTE [90]. Table 5 presents the globally recognized satellite-based evapotranspiration datasets and provides details on the associated data acquisition methods, spatial resolution, temporal resolution, and temporal coverage. The development of evapotranspiration products has evolved from being based on single MODIS data and the Penman–Monteith equation to incorporating multiple satellites, models, and algorithms. The most recent product is able to provide evapotranspiration data at a spatial resolution of 30 m and a temporal resolution of 1 day.

Table 5. Summary of typical satellite-based evapotranspiration datasets.

Dataset	Method	Spatial Resolution	Temporal Resolution	Temporal Coverage
GLEAM	Priestley–Taylor formula based on VOD	1 km	8 d	1980~2021
GLASS_v4	Bayesian model averaging method	1 km	8 d	1981~2021
PLSH	penman-monteith equation	0.08°	1 month	1982~2013
MTE	Multi-mode integration	0.08°	1 month	1982~2016
MOD16	improved penman-monteith equation	500 m	8 d	2000~present
BESS-STAIR	Landsat and MODIS data merging	30 m	1 d	2000~2017
FLUXCOM	Machine learning algorithms based on MODIS and meteorological data	0.5°	8 d	2001~2015
SSEBop	SSEB model based on MODIS and Landsat data	1 km	8 d	2003~present

It is not easy to evaluate satellite evapotranspiration data on a global scale due to the lack of reliable and consistent ground-based observation data [91]. However, many scholars have conducted validations and inter-comparisons of different satellite evapotranspiration products on a regional or basin scale. Previous studies related to the evaluation and intercomparison of these data products were reviewed here to enhance the understanding of

data quality and challenges [92]. Table 6 presents a summary of author names, data sources, study areas, and major conclusions from the corresponding reviewed studies. Overall, the accuracy of each evapotranspiration product varies in different parts of the world. The table indicates that the selection of satellite evapotranspiration products should be carefully conducted based on the existing research and the climatic and geographical characteristics of the study area. Moreover, it is worth noting that the satellite and model merging-based product such as BESS, MTE, and SSEBop tend to generate more precise evapotranspiration estimates compared to the single Mod16 dataset. Hence, incorporating multiple sources of information is essential to improving regional evapotranspiration estimations.

Table 6. Evaluation and inter-comparison of different satellite-based evapotranspiration products over different regions.

Study	Data	Area	Conclusions
[93] (2018)	MOD16	Northwestern Mexico	The MOD16 ET product showed a good correlation with the eddy covariance measurements, but with a significant underestimation. The MOD16 ET product was more accurate in winter than in summer.
[94] (2020)	MOD16/ GLEAM	Australia	AWRA-L ET followed by GLEAM agreed best with flux tower measurements over Australia. AWRA-L and GLEAM outperformed GLDAS and MOD16 ET over forest biome.
[95] (2021)	GLEAM	Iran	GLEAM, ERA5, and GLDAS datasets were more suitable for estimating ET for arid rather than humid basins in Iran and provided better ET estimates in hyper-arid and arid regions from central to eastern Iran than in the humid areas.
[96] (2021)	SSEBop/ MOD16	Europe	Both MOD16 and SSEBop products showed a similar relationship with ground observations, but neither was accurate enough to be a robust basis for studying ET changes in the Alps. The study also identified discrepancies in trends and low correlations between ET and climate variables.
[97] (2021)	PLSH/ MTE/ GLEAM/ MOD16	United States	GLEAM, PLSH, and PML showed the best performance on a yearly scale, while PLSH outperformed others on a seasonal scale. Combining artificial intelligence algorithms or data-driven algorithms with physical process algorithms could further improve the accuracy of ET estimation algorithms and their capacity to be applied in different climate regions.
[98] (2021)	GLASS	Ganjiang Basin, China	Model parameters calibrated by all selected ET datasets produced satisfactory results in streamflow simulations, but the quality was dependent on the calibration schemes and accuracy of ET datasets.
[99] (2022)	GLASS/ MOD16/ GLEAM	Haihe Basin, China	The GLASS_ET data had the smallest average deviation (BIAS) value. The GLEAM_ET data had higher accuracy. The low values of MOD16_ET were overestimated and the high values were underestimated. Most of the ET products had higher R values in spring and lower R values in summer, and the RMSD values of most of the products were highest in summer.
[100] (2022)	BESS/ MOD16/ GLEAM/ SSEBop	South America	The results indicated that while most of the datasets tended to overestimate, there were moderate correlations and similar errors when compared with ET estimated from water balance. However, improvements are needed mainly in the humid tropics to achieve lower uncertainties and higher accuracy of ET estimates for water resource management purposes.

Table 6. *Cont.*

Study	Data	Area	Conclusions
[101] (2022)	GLEAM/ FLUXCOM	East China	Incorporating ET data into all three Scheme II variants was able to improve the performance of extreme flow simulations (including extreme low and high flows). PML could be utilized for multi-variable calibration in drought forecasting, and FLUXCOM and GLEAM were good choices for flood forecasting.
[12] (2022)	GLASS/ BESS/ MOD16	Mekong River Basin, Southeast Asia	MOD16 did not perform well as compared to the other products. The performance of each product varied across different vegetation types. ET ranges of these four products showed great differences in croplands, grasslands, and shrubs. None of the four ET products showed either a consistent temporal trend nor a uniform spatial distribution.

Current satellite-based evapotranspiration products typically exhibit a temporal resolution ranging from monthly to ten-day intervals, accompanied by a spatial resolution exceeding 10 km. Figure 3 shows the global distribution of evapotranspiration derived from the MOD16 product. However, for the development of a digital twin basin, it is necessary to acquire evapotranspiration data at a daily or hourly resolution. Therefore, enhancing the temporal and spatial resolution represents a critical objective in remote sensing evapotranspiration estimation for digital twin basin construction. To accomplish this goal, researchers have undertaken a lot of investigations. For instance, Yao et al. [102] proposed the Taylor merging algorithm, which integrates five Landsat evapotranspiration products with eddy covariance measurements to generate a global evapotranspiration product at a 30 m resolution. Ke et al. [103] employed machine learning algorithms to downscale existing remote sensing products, achieving a spatial resolution of 30 m and a temporal resolution of 8 days.

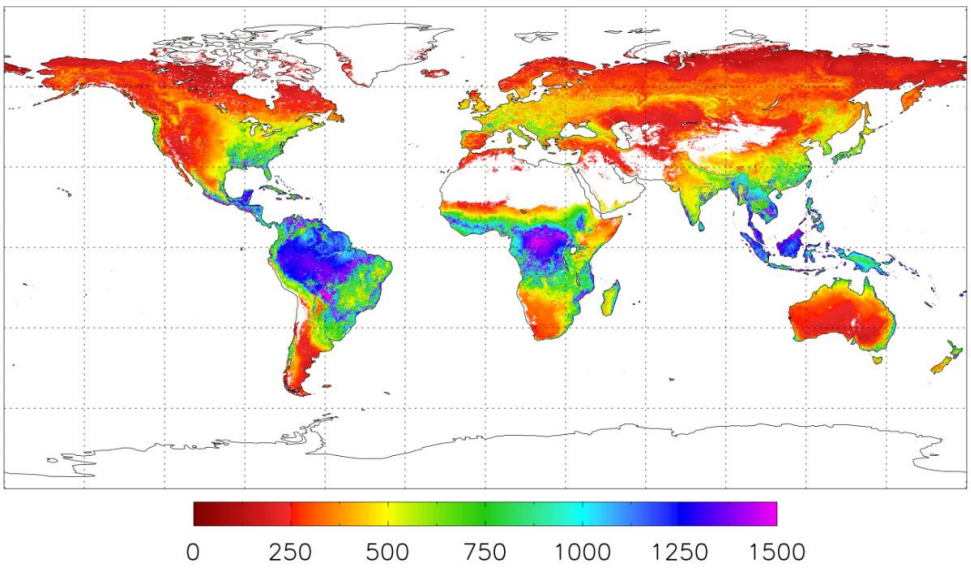

Figure 3. Global evapotranspiration distribution from MOD16 product (mm/year).

In conclusion, satellite-based evapotranspiration estimates offer significant potential for digital twin basin construction, especially in areas where meteorological and underlying surface data are limited. However, the temporal and spatial resolutions of satellite evapotranspiration still cannot satisfy the requirement of various digital twin basin functions, such as flood forecasting. Consequently, greater emphasis should be placed on techniques

such as data assimilation, data merging, and the development of high-resolution algorithms in order to address this issue. Additionally, the underlying surfaces of diverse river basins undergo frequent changes throughout the year, often due to intense human activities. Therefore, the acquisition of precise data pertaining to land cover, vegetation, and albedo is crucial to improving the accuracy of evapotranspiration estimates [104].

3.4. Water Level

The water level of rivers and lakes represents a crucial variable in various fields, including hydrology, water resource management, water conservancy, port and channel design, and other related disciplines. Additionally, it plays a pivotal role as the primary monitoring element in flood forecasting and water resource management, which are among the most vital functions in the application of digital twin basins [105]. Water gauge-based observations at hydrological stations represent the most direct and accurate method for measuring water levels. Through advancements in water conservancy information technology and wireless transmission, automatic water level gauges enable real-time monitoring of specified sections and facilitate data reporting [106]. However, the density of water level monitoring stations in western China, specifically in the Qinghai-Tibet Plateau and Northwest China, is significantly lower than in eastern China. Consequently, this disparity poses challenges in hydrological simulations and forecasting within these regions, as well as obstacles in the construction of a digital twin basin.

In recent years, satellite altimetry technology has been employed to monitor the water levels of rivers and lakes. The principle involves calculating the vertical distance between the satellite and the water surface, thus determining the water level elevation using the satellite's sensor, which receives the reflection signal from the water surface [107]. By observing the difference in height between sea level and the satellite's altimeter, the elevation of the water surface at the satellite's current position can be determined, taking into account the difference between sea level and the geocentric radius of the earth ellipsoid. Several altimetry satellites have been launched, such as the Jason_1, Jason_2, and Jason_3 series launched by NASA and CNES since 2001, the Sentinel series launched by ESA since 2014, and the ICEsat satellites launched by NASA in 2003 and 2018. China has also launched the HY-2A, HY-2B, HY-2C, and HY2-D marine series satellites since 2011, equipped with sensors such as radar altimeters and microwave radiometers, enabling all-weather, continuous, and high-frequency monitoring of the global ocean and land environments [108]. Numerous researchers have conducted studies in various fields based on satellite altimetry data. For example, Wang et al. [109] assessed the accuracy of water level data obtained through Jason_2 satellite altimetry by comparing it with water levels measured using hydrological gauges. The results demonstrated that satellite-based water levels displayed similar trends to actual water level values in the middle Yangtze River. Zhang et al. [110] utilized ICEsat satellite altimetry data to establish time series of lake water levels for lakes in the Qinghai-Tibet Plateau from 2003 to 2009 and from 2018 to the present. They developed a relationship between the lake water level and lake area by incorporating Landsat-observed lake area sequence data. This allowed them to estimate and reconstruct the lake water level sequence for the Qinghai-Tibet Plateau from 1970 to the present. Therefore, satellite altimetry technology serves as an effective auxiliary method for spatial and temporal interpolation and enhancement of water level data in both gauged and ungauged basins. Table 7 presents a summary of key details regarding typical altimetry satellites, including their names, launch organizations, sensor types, satellite altitudes, data accuracy, temporal resolution, and coverage.

Table 7. Summary of typical altimetry satellites.

Satellite	Institution	Sensor	Satellite Altitude	Data Accuracy	Temporal Resolution	Temporal Coverage
ERS-1/2	ESA	Radar altimeter RA/AMI/ATSR-2	782 km	10 cm	35 d	1991~2011
Topex	CNES/ NASA	Poseidon altimeter PA/AMR	1336 km	10 cm	16 d	1993~2005
Jason-1/2/3	CNES/ NASA	Poseidon altimeter/JMR	1336 km	3.3 cm	10 d	2002~present
Cryosat-2	ESA	Interference radar altimeter SIRAL	717 km	4 cm	30 d	2011~present
HY-2A/2B/2C/2D	CNSA	Radar altimeter/laser range finder	971 km	4 cm	10 d	2011~present
Sentinel-3A/3B	ESA	Synthetic aperture radar altimeter	814 km	4 cm	27 d	2016~present
SWOT	NASA	Radar altimeter	891 km	2 cm	11 d	2022~present

Water level observations based on altimeter satellites has made it possible to perform runoff simulations and flood forecasting in ungauged regions as well as achieve continuous observations of lakes and reservoirs with low-cost. However, several scientific challenges must be addressed while applying satellite altimetry data to create digital twin basins. Firstly, it is essential to develop an algorithm for water level estimation according to the characteristics of the terrain, land cover, and data frequency. For instance, Mo [111] employed an adaptive waveform re-tracking method to rectify errors caused by noise effects in altimetry waveforms around detected objects. Additionally, satellite altimetry data precision in the Hongze Lake area was enhanced using a data quality screening method. Secondly, it should be noted that satellite altimetry currently requires water bodies with a width greater than 300 m in order to obtain water level measurements. This implies that only large rivers and lakes are suitable for such measurements. The launch of more advanced fully focused synthetic aperture radar could enable higher-resolution water level measurements for rivers, lakes, and reservoirs [112]. The SWOT (Surface Water and Ocean Topography) satellite, launched in December 2022, will provide global water surface elevation measurements for rivers wider than 100 m and lakes with widths of 250 m by 250 m, with an impressive 2 cm error level. The launch of this satellite heralds a new era of comprehensive and continuous advancements in the field of global hydrology. https://swot.jpl.nasa.gov/ (accessed on 18 December 2022).

Table 8 presents the detailed information of relevant studies for developing altimetry satellite algorithms over different regions, including author names, data sources, study areas, and major conclusions from the corresponding reviewed studies. Although satellite altimetry technology offers data in ungauged basins, current missions primarily focus on subsatellite water bodies, resulting in limited monitoring capabilities for certain lakes and reservoirs with low sampling frequencies. The implementation of multiple altimetry missions will significantly enhance the lake water level database, rectifying this deficiency.

Satellite altimetry technology plays a pivotal role in providing essential data support for hydrological simulation, particularly in regions with limited data availability. However, it is worth noting that certain river basins currently face limitations in utilizing this technology due to inadequate satellite coverage. Fortunately, with the continuous launch of additional satellites, this coverage gap is gradually being addressed, and the potential of satellite altimetry in these areas will be realized. The research and development of convenient, rapid, and efficient data processing methods, such as machine learning-based waveform classification extraction and re-tracking, form a crucial foundation for utilizing vast height measurement data and represent a fundamental research direction in the field of height measurement.

Table 8. Evaluation of altimetry satellite algorithms over different regions.

Study	Data	Area	Conclusions
[113] (2010)	ERS-2	Amazon Basin	Ice-2 and Ice-1 tracking algorithms in the ENVISAT data performed almost equally well. ENVISAT altimetry was clearly an improvement over ERS-2 altimetry.
[114] (2015)	Cryosat-2	Ganges–Brahmaputra River Basin	A key concern for the CryoSat-2 orbit has been its long repeat period of 369 days, which is usually undesirable for river and lake monitoring. The CryoSat-2 data could indeed be used for such monitoring by utilizing the high spatial coverage and sub-cycle period of 30 days.
[115] (2015)	HY-2A/2B/2C/2D	Global	The statistical results from single- and dual-satellite altimeter crossover analysis demonstrated that HY-2A fulfilled its mission requirements (a mean relative bias of −0.21 cm with respect to Jason-2, and a standard deviation of 6.98 cm from dual-satellite crossover analysis). The wavenumber spectra of HY-2A and Jason-2 sea-level anomalies showed similar spectral content, verifying the performance of HY-2A altimetry to be similar to that of Jason-2. Open issues and the remaining HY-2A data problems were identified, allowing prospective future studies to achieve further improvement of its accuracy.
[116] (2016)	ERS-2	West Africa/ Amazon Basin	Low bias and RMSE values for altimeter heights and backscattering were found between ENVISAT and ERS-2 over ocean and flat areas over land and ice sheets with generally better results obtained using CTOH data. Comparisons with in situ water stages also showed good agreement for Ice-2 and especially Ice-1 retracker-derived water levels ($R > 0.95$).
[117] (2018)	Cryosat-2	Po River, Italy	The small across-track distance of CryoSat-2 means that observations are distributed almost continuously along the river. This allowed resolving channel roughness with higher spatial resolution than possible with in situ or virtual station altimetry data. Despite the Po River being extensively monitored, CryoSat-2 still provided added value thanks to its unique spatiotemporal sampling pattern.
[118] (2019)	Sentinel-3A/3B	Global	Computed a new local mean sea surface (MSS) model along the Sentinel-3A ground track. The improvement observed on Sentinel-3A sea level anomalies (SLA) was significant: the residual error was 0.2 cm^2, i.e., 17% of the SLA variance between 15 and 100 km, or 57% less than the gridded MSS model error.
[119] (2020)	Sentinel-3A/3B	Australian coastal region	Sentinel-3A could provide precise SLAs at finer spatial scales. The quality of Sentinel-3A SLAs was superior to that of the retracked Jason-3 dataset in terms of smaller STDs at crossover points (8.8 cm vs. 10.7 cm).
[120] (2022)	Jason	Caspian Sea	To reduce the noise level in Jason altimeter waveforms, singular spectrum analysis (SSA), empirical mode decomposition (EMD), and the combination of SSA and EMD were used to obtain the denoised waveforms. Using the combined denoising method to reduce the noise level was beneficial to improving the accuracy of the MSSH model.
[121] (2022)	Sentinel-3A/3B	Southern coastal waters of Vietnam	Successful retrieval demonstrated the potential for daily monitoring when combining observations from S-3A/B to further improve our understanding of the spatiotemporal dynamics of coastal ecosystems.

Table 8. *Cont.*

Study	Data	Area	Conclusions
[122] (2023)	TOPEX	Global	The main component of the measurement correction resolved the optical phase center variations of the T/P LRA. In addition, systematic station range biases and, to a small extent, geophysical effects were considered. The latter effect was minimized and averaged out by using SLR observations from the entire mission lifetime for the determination of the correction function (with the overall root mean square of SLR residuals of 1.97 cm).
[123] (2023)	Sentinel-3A/3B	Songhua River Basin, Northeast China	The performance of Sentinel-3A altimetry in the Songhua River Basin was not poor. It confirmed that a near-parallel orientation of the river with respect to the satellite ground track often led to poorer performance at virtual stations. If one is aiming to calibrate a hydrodynamic or hydrological model by combining altimetry, VSs with near-parallel orientation are not necessary to be considered when the percentage of the non-parallel crossings of all crossings is big enough.

3.5. River Discharge

River discharge is a crucial variable in real-time flood forecasting, water resource management, river ecosystem protection, and other related fields. It is highly indicative in various assessment areas, such as climate change, water security, and socioeconomic aspects [124]. However, accessing discharge data is usually challenging as it is typically managed by government agencies. In addition, obtaining discharge data in areas without hydrological stations can be difficult [125]. Recently, advances in sensors and computer vision algorithms have emerged as a new approach for measuring river discharge [126]. River discharge measurement can be categorized into two types based on different remote sensing techniques: satellite remote sensing and unmanned aerial vehicle (UAV) measurements.

Satellite remote sensing-based river discharge measurement offers several advantages, including cost-effectiveness and the ability to provide continuous and global measurements regardless of weather conditions [127]. The principle involves extracting essential parameters from satellite imagery, such as river width, water level, and water surface area, based on optical and microwave remote sensing techniques. These parameters are then utilized to establish empirical models that relate river discharge to the extracted parameters. By calibrating these models, river discharge can be accurately estimated [128]. For instance, Majin et al. [129] developed an empirical model for the Heihe River using Landsat satellite data, demonstrating a high correlation coefficient (above 0.9) between estimated and measured discharge. Similarly, Chen et al. [130] proposed a method based on SPOT5 remote sensing images and digital elevation models (DEMs) to estimate discharge in the Dongjiang River Basin. On a global scale, Lin et al. [131] devised a fusion framework incorporating site observations, model simulations, and satellite data. The framework employed machine learning algorithms to reconstruct runoff volume for approximately 2.94 million rivers, achieving a resolution of 0.1° and a sequence length spanning approximately 35 years.

However, satellite remote sensing-based river discharge still encounters several scientific challenges. Firstly, it is limited to rivers with widths exceeding the coverage range (typically 100 m) of satellite sensors. Secondly, the revisit period of satellite passes is typically longer than 3 days. Both challenges result in limitations for applications such as hourly flood forecasting in small river basins [132]. Thirdly, the complex morphology of rivers, including meandering, braiding, and changing river widths, can introduce uncertainties in satellite-based discharge measurements, making it challenging to obtain accurate and consistent results. However, the launch of the SWOT satellite in December 2022 holds promise

for significant advancements in this field. As the world's first specialized water-monitoring satellite, SWOT incorporates wide-width altimetry technology, enabling high-resolution dynamic monitoring of rivers, lakes, reservoirs, and oceans globally. Notably, SWOT offers five times greater target data accuracy than previous observation satellites, such as JASON, facilitating breakthroughs in satellite remote sensing-based discharge measurement. Furthermore, future developments in new sensors, continuous retrieval algorithm optimizations, and multi-data assimilation technology are expected to further enhance the capabilities of satellite-based river discharge measurement [133].

River discharge measurement using unmanned aerial vehicles (UAVs) has witnessed rapid development in recent years. This technology can be classified into image discharge measurement, radar discharge measurement, and video discharge measurement, depending on the sensors employed [134]. Image discharge measurement, similar to satellite remote sensing, benefits from UAVs' enhanced maneuverability and resolution, resulting in higher spatiotemporal resolution data [135]. Radar discharge measurement relies on Doppler radar carried by UAVs, utilizing the Doppler effect. Video discharge measurement utilizes the stereo-vision particle-image method, where water surface flow rate is estimated by extracting features such as floating objects, ripples, and bubbles, followed by tracking matching. River discharge is then calculated based on the river section file [136]. For example, Zhao et al. [137] utilized UAV images and digital surface models (DSMs) to extract point cloud data, allowing for the estimation of river hydraulic parameters and discharge in small watershed areas where measured river section files were unavailable. However, UAV-based river discharge measurement has certain limitations, including reduced measurement accuracy in the absence of floating objects on the river surface and challenges in takeoff during extreme precipitation conditions. Despite these challenges, UAV-based measurements offer several advantages, such as affordability, ease of maintenance, maneuverability, and high accuracy, positioning them as crucial tools in contemporary flood analysis and discharge measurement techniques. More accurate data will be obtained with advancements in image recognition algorithms and UAV technology. Notably, numerous hydrological stations across China have adopted UAV-based discharge measurement as a regular monitoring practice, providing vital data support for digital twin basin construction.

In general, UAV-based river discharge measurement technology has been applied in the real world hydrometry, while satellite-based river discharge measurement technology is still in the development and calibration stage. Improving the accuracy and applicability of satellite remote sensing-based river discharge measurement requires ongoing research and development efforts [138]. Further exploration and refinement of empirical models, integration of diverse data sources, and the utilization of advanced machine learning techniques are essential for enhancing the reliability and spatial coverage of river discharge estimations. Continuous advancements in satellite technology and data processing algorithms will contribute to the broader utilization of satellite remote sensing-based methods for monitoring river flow and supporting the construction of digital twin basins [139].

3.6. Soil Moisture

Soil moisture is among the most active variables in land surface processes [140]. It plays a crucial role in controlling various atmosphere–land surface hydrological fluxes and energy processes, such as precipitation distribution, evapotranspiration, runoff, infiltration, and numerous biotic and ecological processes [141]. Soil moisture serves as a primary focus variable in research fields such as hydrology, ecology, and agriculture, acting as a vital link for interdisciplinary studies. Its wide-ranging applications include land surface hydrological process simulation, water resource management, environmental ecological process simulation, and agricultural irrigation research [142,143]. Consequently, accurate estimation of soil moisture becomes indispensable in the development of digital twin basins.

Currently, three primary methods are employed to acquire soil moisture: in situ measurement, model simulation, and satellite remote sensing-based retrieval [144]. In

situ measurement stands as the most accurate approach utilized by key soil moisture stations in water conservancy and by agriculture departments. However, this method is complex, time-consuming, and impractical for large-scale monitoring [145]. Hydrological models serve as valuable tools for simulating hydrological cycle processes. Advancements in model structures, parameterization schemes, and data accuracy have enabled these models to offer high-precision, large-scale, and spatiotemporal continuous soil moisture estimates [146,147]. However, the accuracy of model simulations can be influenced by factors such as the precision of driving data and the model itself. For instance, Wu et al. [148] discovered that the absence of an irrigation module led to lower simulation accuracy of soil moisture in irrigated areas compared to that in other regions using the variable infiltration capacity (VIC) model. Figure 4 illustrates the spatial distribution of soil moisture obtained using the three data sources, i.e., in situ measurements, SMAP, and VIC, demonstrating a general similarity. The figure demonstrates that satellite remote sensing-based retrieval of soil moisture encounters spatial coverage limitations, particularly in capturing data from snow-covered areas. In addition, the inter-comparison also demonstrates that overall retrieval values are lower than in situ measurements and model data.

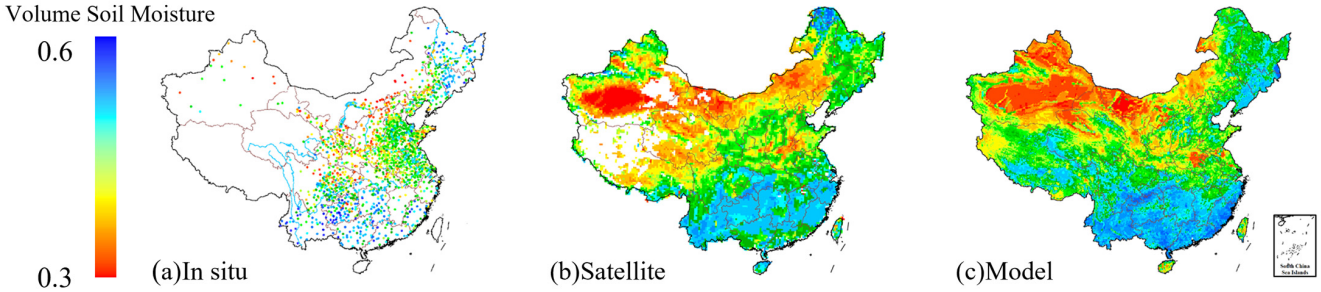

Figure 4. Distribution map of annual averaged soil moisture based on (**a**) in situ measurements, (**b**) satellite remote sensing-based retrieval, and (**c**) model simulation.

The recent advances in microwave remote sensing technology have facilitated the accurate monitoring of soil moisture over large areas [149]. Unlike optical remote sensing, which is susceptible to atmospheric conditions, clouds, and precipitation, microwave remote sensing utilizes longer wavelengths and possesses strong penetration capabilities through vegetation and soil. It can penetrate up to 5 cm below the surface and enables all-day and all-weather monitoring, thus emerging as the most promising technique for quantitative soil moisture sensing [150]. Soil moisture retrieval through microwave remote sensing involves establishing a relationship between soil dielectric properties and soil moisture content. The representative algorithms of satellite-based soil moisture retrieval include single channel algorithm, dual channel algorithm, Land parameter retrieval model, etc. Prominent soil moisture products derived from microwave remote sensing include SMAP (Soil Moisture Active Passive), SMOS (Soil Moisture and Ocean Salinity), and CCI (Climate Change Initiative) [151,152]. Table 9 provides a comprehensive summary of the prevailing satellite-based soil moisture products, including the product names, satellite platforms, launching agencies, sensors, bands, inversion algorithms, spatial resolution, temporal resolution, and temporal coverage.

It is essential to validate and evaluate satellite-based soil moisture products before their utilization due to the uncertainties associated with retrieval algorithms and environmental effect factors [153]. Numerous scholars have conducted evaluation and inter-comparison studies to assess the accuracy of different remote sensing products across various regions worldwide [154,155]. Table 10 provides a summary of these studies, presenting key information such as data sources, regions, and notable findings. This compilation serves as a valuable reference for selecting appropriate satellite soil moisture data in different regions. Among these products, SMAP and CCI demonstrate high accuracy in capturing the temporal trends of real soil moisture patterns across diverse regions globally. The long

time series of CCI data is particularly suitable for climate change research, while SMAP is well-suited for applications such as drought monitoring. Although SMOS data is susceptible to radio frequency interference (RFI), the subsequent implementation of improved retrieval algorithms (SMOS-IC) has significantly enhanced the data quality [156,157].

Table 9. Summary of typical satellite-based soil moisture products.

Product	Satellite	Institution	Sensor	Band	Retrieval Algorithm	Spatial Resolution	Temporal Resolution	Temporal Coverage
SSM/I	DMSP	NOAA	Passive	K band 19.3 Ghz	LPRM	69 × 43 km	3 d	1987~2007
AMI-WS	ERS	ESA	Active	C band 5.3 Ghz	WARP	50 × 50 km	3 d	1991~2006
TMI	TRMM	NASA	Passive	X band 10.7Ghz	LPRM	59 × 36 km	3 d	1997~2015
AMSR-E	Aqua	JAXA	Passive	C/X band 6.9 Ghz/ 10.7 Ghz	Dual-channel retrieval algorithm	76 × 44 km	3 d	2002~2011
AMSR2	GCOM-W1	JAXA	Passive	C/X band 6.9 Ghz/ 10.6 Ghz	Dual-channel retrieval algorithm	35 × 62 km	3 d	2012~present
Windsat	Coriolis	NOAA	Passive	C/X band 6.8 Ghz/ 10.6 Ghz	Multipolar maximum likelihood estimation	25 × 35 km	3 d	1997~2012
ASCAT	MetOp	ESA	Active	C band 5.3 Ghz	Channel detection algorithm	25 × 25 km	3 d	2007~present
SMOS	SMOS	ESA	Passive	L band 1.4 Ghz	Dual-parameter iterative algorithm L-MEB	40 × 40 km	3 d	2009~present
SMAP	SMAP	NASA	Active/ passive	L band 1.4 Ghz	Single-channel polarization Algorithm SCA	36 × 36 km	3 d	2015~present
Sentinel	Sentinel	ESA	Active	C band 5.4 Ghz	Machine learning algorithm	1 × 1 km	3 d	2015~present
CCI	FY/SMOS/ AMSR/ ASCAT	ESA	Active/ passive	Multi-band 1.4 Ghz, 5.3 Ghz, 10.7 Ghz	TC-based merging algorithm	0.25° × 0.25°	1 d	1978~2022

Table 10. Evaluation and inter-comparison of different satellite-based soil moisture products over different regions.

Study	Data	Area	Conclusions
[23] (2015)	CCI/ ASCAT/ AMSR-E	Global	The CCI quality showed an upward trend over time, but a consistent decrease of all performance metrics was observed for the period 2007–2010. The evaluation was conducted using ISMN globally. The data quality of CCI products (with R of 0.46 and RMSE of 0.05) was better than that of other products, except ASCAT. The possible reason for this result was the re-scale algorithm during data merging.
[158] (2016)	SMOS/ ASCAT/ AMSRE	Global	Global comparison indicated that SMOS behaved well compared to AMSRE/ASCAT/ECMWF soil moisture and gave consistent results over all surfaces from very dry (African Sahel, Arizona) to wet (tropical rain forests). RFI (radio frequency interference) was still an issue even though detection had been greatly improved through the significant reduction of RFI sources in several areas of the world.
[159] (2017)	SMAP/ AMSR2	United States	SMAP soil moisture retrieval was generally better than AMSR2 soil moisture data. The remote sensing-based retrievals showed the best agreement with in situ measurements over the central Great Plains and cultivated crops throughout the year. In particular, SMAP soil moisture data showed a stable pattern for capturing the spatial distribution of surface soil moisture.
[160] (2017)	AMSR2/ AMSR-E	Australia	Both AMSR2 C- and X-band SM products were found to show similar temporal patterns and spatial agreement with AMSR-E C- and X-band SM. Despite advances in AMSR2 technology, including superior radiometric sensors and spatial resolution, there were no substantial differences found in LPRM retrievals at resolutions of 1/2° × 1/2° compared to AMSR-E.

Table 10. *Cont.*

Study	Data	Area	Conclusions
[161] (2018)	SMAP/ SMOS/ ASCAT	Global	The evaluation was based on triple collocation-based analysis. It showed the advantage of SMAP (with a global average anomaly correlation of 0.76) over SMOS (0.66) and ASCAT (0.63). In over 50% of retrievals, SMAP had the optimal performance. In North America, Europe, Southern Asia, and eastern Australia, SMAP and SMOS outperformed ASCAT. ASCAT's overall retrieval was better than SMAP and SMOS in high-latitude regions of Eastern Asia, certain parts of South America (primarily Argentina), and southwestern Australia. In western United States, Central Asia, and the majority of internal pixels in eastern Australia, SMOS showed greater R values than SMAP.
[162] (2018)	AMSR2/ AMSR-E/ SMOS/ CCI	Global	CCI_C performed better than both CCI_A and CCI_P considering the temporal variation tendency and absolute value. The ascending data (AMSR_A, SMOS_A) generally outperformed the corresponding descending data (AMSR_D, SMOS_D). AMSR exceeded SMOS in terms of the coefficient of correlation.
[163] (2019)	CCI/ SMOS	Spain	The combined CCI and SMOS SM products matched very well, although SMOS and CCI underestimated and overestimated ground soil moisture measurements, respectively. Merging SMOS in the CCI database could enhance its performance.
[164] (2019)	CCI/SMOS/ SMAP/ AMSR2	Global	The data quality was evaluated based on ISMN. SMAP (ubRMSE = 0.047) and CCI (ubRMSE = 0.041) products were superior to other soil moisture products with advantages in different regions. Compared with the original products of SMOS (ubRMSE = 0.060), the accuracy of SMOS-IC (ubRMSE = 0.048) had been greatly improved, especially in areas with dense vegetation. However, in high VOD, high roughness, topographic complexity and heterogeneity, and tropical or desert regions, soil moisture products still needed to be improved.
[165] (2019)	ASCAT	Global	The performance was evaluated using nine in situ measurement networks. ASCAT predictions overestimated the observed values at all of the sites in Australia. The performance of ASCAT was better in grassland land cover (with R range from 0.46 to 0.90) types.
[166] (2019)	SMAP	Global	The evaluation was conducted based on observations from ISMN. The ubRMSE of SMAP_A and SMAP_P were 0.055 and 0.054, respectfully. Overall, higher accuracy was noted over zones where the soil organic carbon was low, the vegetation density was relatively sparse, locations in the temperate and arid climate zones, and where the mean LST was high. Data quality of SMAP needed to be improved in areas with dense vegetation and low temperature.
[148] (2020)	CCI/ SMOS/ SMAP	China	In general, SMAP was the most reliable product, reflecting the main spatiotemporal characteristics of soil moisture, while SMOS had the lowest accuracy. In irrigated areas, the accuracy of CCI was reduced due to the land surface model used for the rescaling of the CCI_COMBINED soil moisture product during the merging process, while SMAP and SMOS preserved the irrigation signal.
[167] (2020)	Sentinel-1	India	The modified Dubois model provided a good estimate of soil moisture in a region of heterogeneous land cover. The VV polarization of Sentinel-1A was suitable for soil moisture monitoring because the VV polarization was more sensitive to the soil contribution while VH polarization was more sensitive to the vegetation contribution.
[168] (2022)	SMAP/ Sentinel-1	Global	The overall accuracy of SMAP/Sentinel-1 product was acceptable with an average correlation coefficient of 0.67 and ubRMSE of 0.08. The enhanced SMAP product had better performance in estimating SM and a higher actual revisit time than the SMAP/Sentinel-1 product. The accuracy of the SMAP/Sentinel-1 SM product was nearly independent of the presence of water bodies and urban areas, soil texture, and seasonal variation, except the vegetation cover.
[169] (2023)	CCI/SMAP	Tibet, China	The optimal random forest method based on climate, terrain, land cover, and vegetation could improve the accuracy of the original CCI data, which had higher spatiotemporal coverage and closer accuracy than SMAP data.

The application of satellite-based soil moisture into digital twin basins presents several challenges, including the retrieval of root zone soil moisture and the enhancement of soil moisture spatiotemporal resolution to meet digital twin basin requirements. To address these challenges and facilitate the construction of digital twin basins, improvements can be implemented in various ways. One approach is to integrate data from multiple satellite missions, leveraging their respective strengths to improve spatial and temporal resolution. For instance, a joint retrieval technique combining SMAP and Sentinel sensors could produce high-resolution soil moisture data at the 1 km scale [170]. Furthermore, data assimilation techniques should be employed to effectively merge satellite soil moisture observations with hydrological models, remote sensing data, and in situ measurements, enabling more accurate and comprehensive hydrological assessments such as root zone soil moisture retrieval [171]. Finally, the development of new algorithms, such as machine learning, holds promise for integrating satellite soil moisture data with other pertinent environmental variables, including precipitation, temperature, topography, and land cover, to improve soil moisture retrieval [172,173].

3.7. Vegetation

Vegetation data is a focal point of research in diverse disciplines, including hydrology, ecology, climatology, and agronomy. It serves as a fundamental variable for analyzing drought, land cover change, climate change assessment, and evaluating soil erosion [174]. The availability of high-resolution and high-precision vegetation data is crucial for the construction of digital twin basins [175].

Remote sensing vegetation indices are highly effective in acquiring vegetation characteristics of underlying surfaces [176]. Various techniques are employed for vegetation classification, including supervised and unsupervised classification, decision tree, artificial neural networks, support vector machine, deep learning, and reinforcement learning [177,178]. With advancements in quantifying vegetation parameters, a wide range of vegetation indices have been developed for different applications, such as the normalized difference vegetation index (NDVI), enhanced vegetation index (EVI), leaf area index (LAI), and vegetation optical depth (VOD) [179,180]. Currently, the most widely used satellites for vegetation parameter retrieval are the MODIS, Landsat, SPOT, and GF satellite series. Table 11 provides a summary of information on typical satellite-derived vegetation products, including satellite names, launching agencies, sensor types, spatial resolution, temporal resolution, and temporal coverage. However, as highlighted by Zhao et al. [181], remote sensing-based vegetation retrieval still encounters challenges such as pixel mixing, scale effects, errors in physical models, and parameter uncertainties. Therefore, research efforts should be directed towards the development of multi-source and multi-method merging techniques.

Table 11. Summary of typical satellites for vegetation retrieval.

Satellite	Institution	Sensor	Spatial Resolution	Temporal Resolution	Temporal Coverage
Terra/Aqua	NASA	MODIS	1 km	8 d	2000~present
Landsat7	NASA	ETM+	30 m	8 d	2000~present
Landsat8/9	NASA	OLI/TIRS	15 m	8 d	2013~present
SPOT6/7	CNES	Astrium	1.5 m	26 d	2012~present
Sentinel-2A	ESA	Full spectrum imager	10 m	5 d	2015~present
GF-2	CNSA	Panchromatic camera	1 m	69 d	2015~present

Retrieving vegetation parameters from satellite data is the predominant approach for acquiring large-scale and long-term vegetation characteristics [178]. However, it poses challenges in meeting the requirements of spatial resolution, temporal resolution, and data accuracy for field-scale monitoring, such as crop growth monitoring [182]. As a result, researchers have increasingly explored the utilization of unmanned aerial vehicle (UAV)

remote sensing technology for land surface vegetation monitoring [183,184]. For instance, Cao et al. [185] developed a rice leaf area index (LAI) monitoring model in the town of Jiebu using high-resolution UAV images, analyzing the correlation between rice LAI and UAV images at different growth stages. In another study, Chen et al. [186] effectively estimated vegetation coverage in Wendeng county by integrating UAV and remote sensing data through the pixel dichotomy model. Moreover, satellite-based vegetation monitoring should focus more on data merging, machine learning algorithms, and data assimilation in the future.

4. Conclusions and Discussion

A digital twin basin refers to a digitalized virtual representation of a real-world physical basin, which enables an enhanced understanding of the water cycle, provides real-time forecasting and interaction, and supports precise decision-making. Constructing a digital twin basin poses significant challenges as it requires obtaining essential surface variables with large-scale coverage, all-weather capability, high data accuracy, and high spatiotemporal resolution. The advancements in remote sensing sensor performance, retrieval algorithms, and multi-source information acquisition has made remote sensing a promising technology for retrieving essential variables, including meteorological, hydrological, and vegetation variables. This paper provides a comprehensive review and discussion of the retrieval principles, data status, advantages and challenges, and evaluation and inter-comparison of remote sensing-based retrieval for precipitation, surface temperature, evapotranspiration, water level, river discharge, soil moisture, and vegetation, as well as their applications and prospects in digital twin basin construction. The major conclusions are summarized as follows:

Remote sensing-based retrieval possesses several advantages over traditional ground-based observations, including large-scale coverage, lower representativeness error, and cost-effectiveness. In recent years, advancements in sensor technology and algorithms have significantly improved the accuracy, coverage, and spatiotemporal resolution of remote sensing-based retrieval. Consequently, remote sensing has found wider applications in various fields, such as drought monitoring, precipitation forecasting, and water resource management. Remote sensing facilitates data acquisition for constructing digital twin basins, particularly in regions lacking ground-based stations. However, data validation from previous studies has indicated that the accuracy of remote sensing-based retrieval differs significantly across regions of the world due to various underlying land covers, climate features, and environmental characteristics. This suggests that utilizing unverified remote sensing data may introduce significant uncertainties in some regions. Thus, before applying remote sensing data in a digital twin basin, we should emphasize the importance of data calibration and validation based on reliable reference data, as well as data selection according to the inter-comparison results from previous studies.

In certain applications, such as hourly flood forecasting, hydrological simulation in small basins, and urban precipitation monitoring, significant challenges persist in obtaining key surface variables through satellite remote sensing-based retrieval. These challenges include inadequate temporal and spatial resolutions, as well as considerable time latency. Addressing these challenges effectively requires the utilization of radar technology with higher resolution, flow measurement technology based on unmanned aerial vehicles, the advancement of downscaling algorithms, etc. Furthermore, the increasing number of satellite launches and the accumulation of ground-based observation values provide an opportunity to leverage multi-source observation information. Some river basins already possess the foundations for big data algorithms, emphasizing the need for further development and enhancement of techniques such as multi-source data fusion, data assimilation, data bias correction, machine learning algorithms, and multi-sensor joint inversion. With the launch of satellites in thematic series such as the Sentinel series and FY series, more and more multi-source observation information has become available. At the same time, with the accumulation of observational data, some basins have satisfied the requirements of big

data models. Therefore, more attention should be paid in the future to data merging, data assimilation, bias correction, machine learning algorithms, and multi-sensor joint retrieval.

To improve the availability and reliability of remote sensing data, it is necessary to develop algorithms that can standardize data from different remote sensing sources considering variations in location, observation time, grid scale, and data format. Establishing an integrated data platform is essential, encompassing functions such as data access, data quality control, data standardization, data interface services, and other related features. Additionally, future research should also focus on high performance computing and developing corresponding acceleration algorithms to expedite remote sensing data processing and reduce output delays. These research directions aim to accelerate the application of remote sensing in the construction of digital twin basins.

Author Contributions: Conceptualization, X.W.; methodology, X.W. and Z.W.; formal analysis, X.W. and G.L.; investigation, X.W.; resources, X.W.; writing—original draft preparation, X.W.; writing—review and editing, X.W., G.L. and Z.W.; funding acquisition, X.W. and Z.W. All authors have read and agreed to the published version of the manuscript.

Funding: This research was funded by the Postdoctoral Fund Project of SIDRI grant number 2022SL831-001, the Research Fund Project of SIDRI grant number 2023YF20-001, the National Natural Science Foundation of China grant number U2240225.

Conflicts of Interest: The auhors declare no conflict of interest.

References

1. Grieves, M. Digital Twin: Manufacturing Excellence through Virtual Factory Replication. *White Pap.* **2014**, *1*, 1–7.
2. Li, G.Y. Accelerating the construction of digital twin basins to enhance national water security capabilities. *Water Conserv. Constr. Manag.* **2022**, *42*, 1–2.
3. Cai, Y. Constructing a smart water conservancy system with "four predictions" functions based on digital twin basins. *China Water Resour.* **2022**, *20*, 2–6.
4. Ye, Y.T.; Jiang, Y.Z.; Liang, L.L.; Zhao, H.L.; Gu, J.J.; Dong, J.P.; Cao, Y.; Duan, H. Digital twin basins: A new infrastructure and paradigm for future basin governance and management. *Adv. Water Sci.* **2022**, *33*, 683–704.
5. Huang, Y. Preliminary exploration of key technologies and pilot projects for digital twin Yangtze River. *China Flood Drought Manag.* **2022**, *32*, 11.
6. Liu, C.J.; Lv, J.; Ren, M.L.; Chen, S.; Zhang, X.L.; Song, W.L.; Zhang, D.W. Research and practice of digital twin Huaihe River basin smart flood control system. *China Flood Drought Manag.* **2022**, *32*, 7.
7. Liu, Y.S.; Liu, C.J.; Hao, M.; Song, W.L.; Qu, W.; Chen, S.; Lv, J. Construction of data bottom plate for digital twin basin oriented to "four predictions" flood control. *China Flood Drought Manag.* **2022**, *32*, 6–14.
8. Zeng, G.X.; He, L.H.; Tang, Z.R.; Huo, H.X. Building standard-anchored digital twin basin construction goals based on unified data bottom plate. *China Water Resour.* **2022**, *20*, 38–41.
9. Hu, C.H.; Guo, Q.C.; Zhang, L.; Qin, W.; Guan, J.Z. Some issues to be considered in the development of digital twin basin model. *China Water Resour.* **2022**, *20*, 7–10.
10. Lian, B.; Wei, Z.C.; Zhao, J.J. Review on key technologies and applications of smart water conservancy. *Water Conserv. Informatiz.* **2021**, *5*, 6–18.
11. Xu, Z.H. Application of satellite remote sensing technology in smart water conservancy construction. *China New Commun.* **2020**, *22*, 2.
12. Chen, H.; Gnanamoorthy, P.; Chen, Y.; Mansaray, L.R.; Song, Q.; Liao, K.; Shi, A.; Feng, G.; Sun, C. Assessment and Inter-Comparison of Multi-Source High Spatial Resolution Evapotranspiration Products over Lancang–Mekong River Basin, Southeast Asia. *Remote Sens.* **2022**, *14*, 479. [CrossRef]
13. Amani, M.; Moghimi, A.; Mirmazloumi, S.M.; Ranjgar, B.; Ghorbanian, A.; Ojaghi, S.; Ebrahimy, H. Ocean Remote Sensing Techniques and Applications: A Review (Part I). *Water* **2022**, *14*, 3400. [CrossRef]
14. Zhu, D.J.; Li, H.B.; Wang, X.M. Application prospect of GNSS remote sensing technology in smart water conservancy construction. *Water Resour. Hydropower Eng.* **2022**, *53*, 33–57.
15. Tang, G.Q.; Long, D.; Wan, W.; Zeng, Z.Y.; Guo, X.L.; Hong, Y. A review and prospect on global water remote sensing technology and its application research. *Sci. Technol. Rev.* **2015**, *45*, 1013–1023.
16. Du, M.D. *Study on Hydrological Model Based on Multi-Source Remote Sensing Data in Data-Deficient Areas*; Tsinghua University: Beijing, China, 2018.
17. Zhang, A.Z. Monitoring meteorological drought in semiarid regions using multi-sensor microwave remote sensing data. *Remote Sens. Environ.* **2013**, *134*, 12–23. [CrossRef]

18. Song, P.; Liu, Y.B.; Liu, Y.C. Research progress of satellite remote sensing inversion of land surface water parameters. *Adv. Earth Sci.* **2011**, *26*, 10.
19. Chao, L.; Zhang, K.; Wang, S.; Gu, Z.; Xu, J.; Bao, H. Assimilation of surface soil moisture jointly retrieved by multiple microwave satellites into the WRF-Hydro model in ungauged regions: Towards a robust flood simulation and forecasting. *Environ. Model. Softw.* **2022**, *324*, 105421. [CrossRef]
20. Lei, B.E.; Wang, S.H. Review on application status of microwave remote sensing. *Sci. Sq.* **2016**, *6*, 171–174.
21. Liu, S.X. *Research on Minute-Level Precipitation Estimation Method in Southwest Mountainous Area Based on Weather Radar and Satellite Data Fusion*; University of Electronic Science and Technology of China: Chengdu, China, 2021.
22. Gruber, A.; Dorigo, W.A.; Crow, W.; Wagner, W. Triple Collocation-Based Merging of Satellite Soil Moisture Retrievals. *IEEE Trans. Geosci. Remote Sens.* **2017**, *55*, 6780–6792. [CrossRef]
23. Dorigo, W.A.; Gruber, A.; Jeu, R.A.M.D.; Wagner, W.; Stacke, T.; Loew, A.; Albergel, C.; Brocca, L.; Chung, D.; Parinussa, R.M. Evaluation of the ESA CCI soil moisture product using ground-based observations. *Remote Sens. Environ* **2015**, *162*, 380–395. [CrossRef]
24. Yu, H.; Zhang, X.T.; Feng, Q.S.; Wang, W.; Wang, Z.W.; Liang, T.G. Research progress on optical and microwave remote sensing of snow in pastoral areas. *Pratacultural Sci.* **2010**, *27*, 10.
25. Ding, B.; Li, W.; Hu, K. Inversion of suspended matter in Maowei Sea and its estuary water body based on synchronous optical and microwave remote sensing. *Remote Sens. Land Resour.* **2022**, *34*, 10–17.
26. Zhu, S. *Classification and Reconstruction of Microwave and Optical Remote Sensing Images*; University of Electronic Science and Technology of China: Chengdu, China, 2017.
27. Wang, K.; Fu, Y.R.; Peng, X.Y.; Zuo, Z.Q.; Yi, L.; Huang, S.B. Progress and typical industry applications of low-altitude remote sensing technology for unmanned aerial vehicles. *Mapp. Surv. Eng. Bull.* **2017**, *1*, 79–83.
28. Fu, H.Y. *Study on Monitoring Land Salinization and Soil Moisture Salt Content Inversion Based on Optical and Microwave Remote Sensing Technology*; Jilin University: Changchun, China, 2020.
29. Fan, L. *Estimation of Soil Moisture and Forest Fire Risk Assessment Based on Multi-Source Data*; Institute of Remote Sensing and Digital Earth Chinese Academy of Sciences (University of Chinese Academy of Sciences): Beijing, China, 2017.
30. Deng, X.D.; Wang, H.Q. Research progress on soil moisture microwave remote sensing inversion algorithm and application. *J. Zhejiang Univ. (Agric. Life Sci.)* **2022**, *48*, 289–302.
31. Li, B.X. *Inversion of Soil Moisture in Farmland Covered by Vegetation Based on Optical and Microwave Remote Sensing Data*; East China University of Technology: Fuzhou, China, 2020.
32. Peng, Z.H.; Li, Y.Z.; Yu, W.J.; Xing, Y.C.; Feng, A.Q.; Du, S.W. Applicability study of remote sensing precipitation products in different climatic regions in China. *J. Geo-Inf. Sci.* **2021**, *23*, 1296–1311.
33. Wang, X.Y.; Lu, F.; Zhu, K.; Zhou, Y.Y.; Wu, Z. Comparison study on multi-time scale of different remote sensing precipitation products—Taking Sanjiangyuan area as an example. *China Rural. Water Hydropower* **2022**, *7*, 132–139.
34. Zhang, H.B.; Dou, S.Q.; Wen, Y.; Xu, Y.; Zhang, N.; Miao, L.L. Spatial downscaling and drought spatiotemporal monitoring of remote sensing precipitation data. *J. Soil Water Conserv.* **2022**, *36*, 8.
35. Gao, Z.; Huang, B.S.; Chen, X.H.; Qiu, J. Multi-source remote sensing precipitation evaluation and its application in hydrological simulation. *China Rural. Water Hydropower.* **2021**, *4*, 27–32.
36. Luo, Y.L. *Drought Monitoring in Xiangjiang River Basin Based on Remote Sensing Soil Moisture and Precipitation*; Southeast University: Dhaka, Bangladesh, 2020.
37. Wang, C.G.; Hong, Y. Review on inversion verification and application of satellite remote sensing precipitation. *Water Resour. Hydropower Eng.* **2018**, *49*, 9.
38. Gosset, M.; Viarre, J.; Quantin, G.; Alcoba, M. Evaluation of several rainfall products used for hydrological applications over West Africa using two high-resolution gauge networks. *Q. J. R. Meteorol. Soc.* **2013**, *139*, 923–940. [CrossRef]
39. Mi, J.W.; Tian, J.Y.; Xue, H.; Qiu, Q.T.; Liu, R.H. Application evaluation of radar rainfall measurement and near-term forecasting in small and medium-sized watersheds from a hydrological perspective. *Sci. Technol. Eng.* **2022**, *22*, 10247–10254.
40. Liu, S.J.; Cai, D.X.; Han, J.; Gan, Y.X. A brief summary of research progress on satellite remote sensing inversion of precipitation. *Adv. Meteorol. Sci. Technol.* **2021**, *11*, 28–33.
41. Islam, M.A.; Yu, B.; Cartwright, N. Assessment and comparison of five satellite precipitation products in Australia. *J. Hydrol.* **2020**, *590*, 125474. [CrossRef]
42. Lu, D.K.; Yong, B. A preliminary assessment of the gauge-adjusted near-real-time GSMaP precipitation estimate over Mainland China. *Remote Sens.* **2020**, *12*, 141. [CrossRef]
43. Alsumaiti, T.S.; Hussein, K.; Ghebreyesus, D.T.; Sharif, H.O. Performance of the CMORPH and GPM IMERG Products over the United Arab Emirates. *Remote Sens.* **2020**, *12*, 1426. [CrossRef]
44. Wang, J. Validation of Satellite-Based Precipitation Products from TRMM to GPM. *Remote Sens.* **2021**, *13*, 1745. [CrossRef]
45. Siddig, M.S.A.; Ibrahim, S.; Yu, Q.; Abdalla, A.; Osman, Y.; Atiem, I.A.; Hamukwaya, S.L.; Taha, M.M.M. Bias Adjustment of Four Satellite-Based Rainfall Products Using Ground-Based Measurements over Sudan. *Water* **2022**, *14*, 1475. [CrossRef]
46. Usman, M.; Ndehedehe, C.E.; Farah, H.; Ahmad, B.; Wong, Y.; Adeyeri, O.E. Application of a Conceptual Hydrological Model for Streamflow Prediction Using Multi-Source Precipitation Products in a Semi-Arid River Basin. *Water* **2022**, *4*, 1260. [CrossRef]

47. Kimani, M.W.; Hoedjes, J.C.B.; Su, Z. An Assessment of Satellite-Derived Rainfall Products Relative to Ground Observations over East Africa. *Remote Sens.* **2017**, *9*, 430. [CrossRef]
48. Ye, X.; Guo, Y.; Wang, Z.; Liang, L.; Tian, J. Extensive Evaluation of Four Satellite Precipitation Products and Their Hydrologic Applications over the Yarlung Zangbo River. *Remote Sens.* **2022**, *14*, 3350. [CrossRef]
49. Salehi, H.; Sadeghi, M.; Golian, S.; Nguyen, P.; Murphy, C.; Sorooshian, S. The Application of PERSIANN Family Datasets for Hydrological Modeling. *Remote Sens.* **2022**, *14*, 3675. [CrossRef]
50. Papacharalampous, G.; Tyralis, H.; Doulamis, A.; Doulamis, N. Comparison of machine learning algorithms for merging gridded satellite and earth-observed precipitation data. *Water* **2023**, *15*, 634. [CrossRef]
51. Guo, B.; Xu, T.; Yang, Q.; Zhang, J.; Dai, Z.; Deng, Y.; Zou, J. Multiple Spatial and Temporal Scales Evaluation of Eight Satellite Precipitation Products in a Mountainous Catchment of South China. *Remote Sens.* **2023**, *15*, 1373. [CrossRef]
52. Gulakhmadov, M.; Chen, X.; Gulakhmadov, A.; Nadeem, M.U.; Gulahmadov, N.; Liu, T. Performance Analysis of Precipitation Datasets at Multiple Spatio-Temporal Scales over Dense Gauge Network in Mountainous Domain of Tajikistan, Central Asia. *Remote Sens.* **2023**, *15*, 1420. [CrossRef]
53. Li, H.Y.; Zhang, Y.; Lei, H.J.; Hao, X.H. Machine Learning-Based Bias Correction of Precipitation Measurements at High Altitude. *Remote Sens.* **2023**, *15*, 2072. [CrossRef]
54. Papacharalampous, G.; Tyralis, H.; Doulamis, A.; Doulamis, N. Comparison of tree-based ensemble algorithms for merging satellite and earth-observed precipitation data at the daily time scale. *Hydrology* **2023**, *10*, 50. [CrossRef]
55. Ming, L.; Shao, Q. An improved statistical approach to merge satellite rainfall estimates and raingauge data. *J. Hydrol.* **2010**, *385*, 51–64.
56. Xu, S.; Wu, C.; Wang, L.; Gonsamo, A.; Shen, Y.; Niu, Z. A new satellite-based monthly precipitation downscaling algorithm with non-stationary relationship between precipitation and land surface characteristics. *Remote Sens. Environ.* **2015**, *162*, 119–140. [CrossRef]
57. Xiong, L.H.; Liu, C.K.; Chen, S.L.; Zha, X.N.; Ma, Q.M. Review of post-processing research on remote sensing precipitation data. *Adv. Water Sci.* **2021**, *32*, 627–637.
58. Tang, G.Q. *Verification, Application and Improvement of Satellite Remote Sensing Precipitation in Global and Typical Regions*; Tsinghua University: Beijing, China, 2019.
59. Sun, Z.L.; Wu, Z.Y.; He, H. Evaluation and correction of TRMM satellite inversion precipitation in typical plain areas of Jiangsu Province. *Water Resour. Power Energy Sci.* **2017**, *35*, 24–28.
60. Zhang, P. *Research on the Application Method of Microwave Link in Weather Radar Quantitative Measurement of Precipitation*; National University of Defense Technology: Changsha, China, 2018.
61. Zou, M.Z.; Chen, Z.L.; Chen, J.; Li, Q.; Wu, H.N. Innovation and application of rainfall measurement technology. *China Water Resour.* **2020**, *20*, 81–83.
62. Ge, L.L. *Research on Remote Sensing Inversion Method for Soil Moisture and Air Temperature Based on Machine Learning*; Nanjing University of Information Science & Technology: Nanjing, China, 2021.
63. Nieto, H.; Sandholt, I.; Aguado, I.; Chuvieco, E.; Stisen, S. Air temperature estimation with MSG-SEVIRI data: Calibration and validation of the TVX algorithm for the Iberian Peninsula. *Remote Sens. Environ.* **2011**, *115*, 107–116. [CrossRef]
64. Hou, Y.Y.; Zhang, J.H.; Yan, H.; Wang, J.L. Estimation of regional-scale air temperature using satellite remote sensing data. *Meteorol. Mon.* **2010**, *4*, 75–79.
65. Renhua, Z.; Yuan, R.; Jing, T.; Hongbo, S.; Zhao-Liang, L.; Suhua, L. A Remote Sensing Method for Estimating Surface Air Temperature and Surface Vapor Pressure on a Regional Scale. *Remote Sens.* **2015**, *7*, 6005–6025.
66. Zhang, L.W.; Huang, J.F.; Wang, X.Z. A review on remote sensing methods for estimating air temperature. *J. Nat. Resour.* **2014**, *29*, 540–552.
67. Leng, P.; Liao, Q.Y.; Ren, C.; Li, Z.L. A review on remote sensing methods for estimating near-surface air temperature. *China Agric. Inf.* **2019**, *31*, 1–10.
68. Yang, Y.Z.; Cai, W.H.; Yang, J. Evaluation of MODIS Land Surface Temperature Data to Estimate Near-Surface Air Temperature in Northeast China. *Remote Sens.* **2017**, *9*, 410. [CrossRef]
69. Choi, Y.; Suh, M. Development of Himawari-8/Advanced Himawari Imager (AHI) Land Surface Temperature Retrieval Algorithm. *Remote Sens.* **2018**, *10*, 2013. [CrossRef]
70. Sekertekin, A.; Bonafoni, S. Sensitivity Analysis and Validation of Daytime and Nighttime Land Surface Temperature Retrievals from Landsat 8 Using Different Algorithms and Emissivity Models. *Remote Sens.* **2020**, *12*, 2776. [CrossRef]
71. Shiff, S.; Lensky, D.H.I.M. Worldwide continuous gap-filled MODIS land surface temperature dataset. *Sci. Data* **2021**, *8*, 74. [CrossRef] [PubMed]
72. Duan, S.; Li, Z.; Zhao, W.; Wu, P.; Huang, C.; Han, X.; Gao, M.; Leng, P.; Shang, G. Validation of Landsat land surface temperature product in the conterminous United States using in situ measurements from SURFRAD, ARM, and NDBC sites. *Int. J. Digit Earth* **2021**, *14*, 640–660. [CrossRef]
73. Li, S.; Wang, J.; Li, D.; Ran, Z.; Yang, B. Evaluation of Landsat 8-like Land Surface Temperature by Fusing Landsat 8 and MODIS Land Surface Temperature Product. *Processes* **2021**, *9*, 2262. [CrossRef]

74. Pérez-Planells, L.; Niclòs, R.; Puchades, J.; Coll, C.; Göttsche, F.-M.; Valiente, J.A.; Valor, E.; Galve, J.M. Validation of Sentinel-3 SLSTR Land Surface Temperature Retrieved by the Operational Product and Comparison with Explicitly Emissivity-Dependent Algorithms. *Remote Sens.* **2021**, *13*, 2228. [CrossRef]
75. Yu, P.; Zhao, T.; Shi, J.; Ran, Y.; Jia, L.; Ji, D.; Xue, H. Global spatiotemporally continuous MODIS land surface temperature dataset. *Sci. Data* **2022**, *9*, 143. [CrossRef]
76. Chen, D.; Zhuang, Q.; Zhu, L.; Zhang, W. Comparison of Methods for Reconstructing MODIS Land Surface Temperature under Cloudy Conditions. *Appl. Sci.* **2022**, *12*, 6068. [CrossRef]
77. Onačillová, K.; Gallay, M.; Paluba, D.; Péliová, A.; Tokarčík, O.; Laubertová, D. Combining Landsat 8 and Sentinel-2 Data in Google Earth Engine to Derive Higher Resolution Land Surface Temperature Maps in Urban Environment. *Remote Sens.* **2022**, *14*, 4076. [CrossRef]
78. Dong, L.X.; Tang, S.H.; Wang, F.Z.; Cosh, M.; Li, X.X.; Min, M. Inversion and Validation of FY-4A Official Land Surface Temperature Product. *Remote Sens.* **2023**, *15*, 2437. [CrossRef]
79. Xu, Y.M.; Qin, Z.H.; Wan, H.X. Research progress in thermal infrared remote sensing inversion near-surface air temperature. *Remote Sens. Land Resour.* **2011**, 9–14.
80. Chen, Y.Y.; Deng, X.B.; Huang, Q.H.; Liu, H.L.; Wang, Y.Z.; Yuan, S.J. Spatiotemporal fusion of temperature based on FY-3D and FY-4A. *J. Chengdu Univ. Inf. Technol.* **2022**, 37.
81. Zhou, J.; Zhao, Y.P.; Yue, T.X.; Lu, T. Estimation of near-surface temperature at provincial scale combining HASM and GWR methods. *J. Geo-Inf. Sci.* **2020**, *22*, 2098–2107.
82. Jung, M.; Reichstein, M.; Ciais, P.; Seneviratne, S.I.; Sheffield, J.; Goulden, M.L.; Bonan, G.; Cescatti, A.; Chen, J.; Jeu, R.D. Recent decline in the global land evapotranspiration trend due to limited moisture supply. *Nature* **2010**, *467*, 951–954. [CrossRef]
83. Zhang, Y.; Jia, Z.Z.; Liu, S.M.; Xu, Z.W.; Xu, T.R.; Yao, Y.J.; Ma, Y.F.; Song, L.S.; Li, X.; Hu, X. Research progress in the verification of remote sensing estimation of surface evapotranspiration. *J. Remote Sens.* **2020**, *24*, 975–999.
84. Wang, K.; Dickinson, R.E. A review of global terrestrial evapotranspiration: Observation, modeling, climatology, and climatic variability. *Rev. Geophys.* **2012**, *50*, 2. [CrossRef]
85. Liu, H.T. *Remote Sensing Inversion and Hydrological Simulation Study on the Impact of Human Activities on Basin Evapotranspiration*; Nanjing University of Information Science and Technology: Nanjing, China, 2022.
86. Meng, Y.; Jiang, P.; Dong, W. Research progress on surface evapotranspiration based on remote sensing. *Remote Sens. Technol. Appl.* **2022**, *37*, 839–853.
87. Chen, L.; Sun, F.F. Calculation of evapotranspiration based on unmanned aerial vehicle remote sensing—Taking key development areas in Longhua District as an example. *Environ. Ecol.* **2022**, *4*, 27–35.
88. Xiong, Y.J.; Feng, F.G.; Fang, Y.Z.; Qiu, G.Y.; Zhao, S.H.; Yao, Y.J. Discussion on key issues in application of remote sensing inversion products for evapotranspiration. *Remote Sens. Technol. Appl.* **2021**, *36*, 121–131.
89. Jiang, C.; Ryu, Y. Multi-scale evaluation of global gross primary productivity and evapotranspiration products derived from Breathing Earth System Simulator (BESS). *Remote Sens. Environ.* **2016**, *186*, 528–547. [CrossRef]
90. Liu, M.; Tang, R.L.; Li, Z.L. Research progress in data-driven remote sensing inversion methods and products for evapotranspiration. *J. Remote Sens.* **2021**, *25*, 1517–1537.
91. Ke, Z.; Kimball, J.S.; Running, S.W. A review of remote sensing based actual evapotranspiration estimation. *Wiley Interdiscip. Rev. Water* **2016**, *3*, 834–854.
92. Xu, T.R.; Guo, Z.X.; Xia, Y.L. Evaluation of twelve evapotranspiration products from machine learning, remote sensing and land surface models over conterminous United States. *J. Hydrol.* **2019**, *578*, 124105. [CrossRef]
93. Aguilar, A.L.; Flores, H.; Crespo, G.; Marín, M.I.; Campos, I.; Calera, A. Performance Assessment of MOD16 in Evapotranspiration Evaluation in Northwestern Mexico. *Water* **2018**, *10*, 901. [CrossRef]
94. Khan, M.S.; Baik, J.; Choi, M. Inter-comparison of evapotranspiration datasets over heterogeneous landscapes across Australia. *Adv. Space Res.* **2020**, *66*, 533–545. [CrossRef]
95. Panahi, D.M. Spatio-Temporal Assessment of Global Gridded Evapotranspiration Datasets across Iran. *Remote Sens.* **2021**, *13*, 1816. [CrossRef]
96. Castelli, M. Evapotranspiration Changes over the European Alps: Consistency of Trends and Their Drivers between the MOD16 and SSEBop Algorithms. *Remote Sens.* **2021**, *13*, 4316. [CrossRef]
97. Chao, L.; Zhang, K.; Wang, J.; Zhang, J.F.A.M. A Comprehensive Evaluation of Five Evapotranspiration Datasets Based on Ground and GRACE Satellite Observations: Implications for Improvement of Evapotranspiration Retrieval Algorithm. *Remote Sens.* **2021**, *13*, 2414. [CrossRef]
98. Guo, X.; Wu, Z.; He, H.; Xu, Z. Evaluating the Potential of Different Evapotranspiration Datasets for Distributed Hydrological Model Calibration. *Remote Sens.* **2022**, *14*, 629. [CrossRef]
99. Guo, X.; Meng, D.; Chen, X.; Li, X. Validation and Comparison of Seven Land Surface Evapotranspiration Products in the Haihe River Basin, China. *Remote Sens.* **2022**, *14*, 4308. [CrossRef]
100. Ruhoff, A.; de Andrade, B.C.; Laipelt, L.; Fleischmann, A.S.; Siqueira, V.A.; Moreira, A.A.; Barbedo, R.; Cyganski, G.L.; Fernandez, G.M.R.; Brêda, J.P.L.F.; et al. Global Evapotranspiration Datasets Assessment Using Water Balance in South America. *Remote Sens.* **2022**, *14*, 2526. [CrossRef]

101. Pan, S.; Xu, Y.; Gu, H.; Yu, B.; Xuan, W. Evaluation of Remote Sensing-Based Evapotranspiration Datasets for Improving Hydrological Model Simulation in Humid Region of East China. *Remote Sens.* **2022**, *14*, 4546. [CrossRef]
102. Yao, Y.; Liang, S.; Li, X.; Zhang, Y.; Chen, J.; Jia, K.; Zhang, X.; Fisher, J.B.; Wang, X.; Zhang, L. Estimation of high-resolution terrestrial evapotranspiration from Landsat data using a simple Taylor skill fusion method. *J. Hydrol.* **2017**, *553*, 508–526. [CrossRef]
103. Yinghai; Gong; Huili; Park; Seonyoung; Jungho Spatiotemporal downscaling approaches for monitoring 8-day 30 m actual evapotranspiration. *ISPRS J. Photogramm. Remote Sens.* **2017**, *126*, 79–93. [CrossRef]
104. Fisher, J.B.; Melton, F.; Middleton, E.; Hain, C.; Anderson, M.; Allen, R.; Mccabe, M.F.; Hook, S.; Baldocchi, D.; Townsend, P.A. The future of evapotranspiration: Global requirements for ecosystem functioning, carbon and climate feedbacks, agricultural management, and water resources. *Water Resour. Res.* **2017**, *53*, 2618–2626. [CrossRef]
105. Pekel, J.F.; Cottam, A.; Gorelick, N.; Belward, A.S. High-resolution mapping of global surface water and its long-term changes. *Nature* **2016**, *540*, 418–422. [CrossRef]
106. Zhang, C.H. *Study on the Estimation Method of Lake Storage Based on Multi-Source Remote Sensing Data*; Shandong Jianzhu University: Jinan, China, 2022.
107. Zhai, G.J.; Huang, M.T.; Ouyang, Y.Z.; Lu, X.P. Satellite altimetry principle and its application. *Hydrogr. Surv. Charting* **2002**, *1*, 57–62.
108. Li, X.; Ling, F.; Foody, G.M.; Boyd, D.S.; Jiang, L.; Zhang, Y.; Zhou, P.; Wang, Y.; Chen, R.; Du, Y. Monitoring high spatiotemporal water dynamics by fusing MODIS, Landsat, water occurrence data and DEM. *Remote Sens. Environ.* **2021**, *265*, 112680. [CrossRef]
109. Wang, H.; Sun, F.B.; Yang, T.; Liu, F. Application of Jason-2 satellite altimetry data in water level monitoring in the middle reaches of the Yangtze River. *Three Gorges Ecol. Environ. Monit.* **2018**, *3*, 48–54.
110. Zhang, G.Q.; Wang, M.M.; Zhou, T.; Chen, W.F. Research progress on remote sensing monitoring of lake area, water level and water volume changes in Qinghai-Tibet Plateau. *J. Remote Sens.* **2022**, *26*, 115–125.
111. Mo, D.L. *Research on Typical Water Level Remote Sensing Monitoring Methods*; Nanning Normal University: Nanning, China, 2021.
112. Yuan, C.; Gong, P.; Bai, Y. Performance Assessment of ICESat-2 Laser Altimeter Data for Water-Level Measurement over Lakes and Reservoirs in China. *Remote Sens.* **2020**, *12*, 770. [CrossRef]
113. Silva, J.; Calmant, S.; Seyler, F.; Filho, O.; Cochonneau, G.; Mansur, W.J. Water levels in the Amazon basin derived from the ERS 2 and ENVISAT radar altimetry missions. *Remote Sens. Environ.* **2010**, *114*, 2160–2181. [CrossRef]
114. Villadsen, H.; Andersen, O.B.; Stenseng, L.; Nielsen, K.; Knudsen, P. CryoSat-2 altimetry for river level monitoring—Evaluation in the Ganges–Brahmaputra River basin—ScienceDirect. *Remote Sens. Environ.* **2015**, *168*, 80–89. [CrossRef]
115. Bao, L.; Peng, G.; Peng, H.; Jia, Y.; Qi, G. First accuracy assessment of the HY-2A altimeter sea surface height observations: Cross-calibration results. *Adv. Space Res.* **2015**, *55*, 90–105. [CrossRef]
116. Frappart, F.; Legrésy, B.; Fernando, N.; Blarel, F.; Fuller, N.; Fleury, S.; Birol, F.; Calmant, S. An ERS-2 altimetry reprocessing compatible with ENVISAT for long-term land and ice sheets studies. *Remote Sens. Environ.* **2016**, *184*, 558–581. [CrossRef]
117. Schneider, R.; Tarpanelli, A.; Nielsen, K.; Madsen, H.; Bauer-Gottwein, P. Evaluation of multi-mode CryoSat-2 altimetry data over the Po River against in situ data and a hydrodynamic model. *Adv. Water Resour.* **2018**, *112*, 17–26. [CrossRef]
118. Gd, A.; Mip, B. Improving the quality of Sentinel-3A data with a hybrid mean sea surface model, and implications for Sentinel-3B and SWOT—ScienceDirect. *Adv. Space Res.* **2019**, *68*, 1116–1139.
119. Peng, F. Validation of Sentinel-3A SAR mode sea level anomalies around the Australian coastal region. *Remote Sens. Environ.* **2020**, *237*, 111548. [CrossRef]
120. Jiang, W.; You, W. A combined denoising method of empirical mode decomposition and singular spectrum analysis applied to Jason altimeter waveforms: A case of the Caspian Sea. *Geod. Geodyn.* **2022**, *13*, 327–342. [CrossRef]
121. Binh, N.A.; Hoa, P.V.; Thao, G.T.P.; Duan, H.D.; Thu, P.M. Evaluation of Chlorophyll-a estimation using Sentinel 3 based on various algorithms in southern coastal Vietnam. *Int. J. Appl. Earth Obs. Geoinf.* **2022**, *112*, 102951. [CrossRef]
122. Zeitlhöfler, J.; Bloßfeld, M.; Rudenko, S.; Dettmering, D.; Seitz, F. Station-dependent satellite laser ranging measurement corrections for TOPEX/Poseidon. *Adv. Space Res.* **2023**, *71*, 975–996. [CrossRef]
123. Chen, J.; Fenoglio, L.; Kusche, J.; Liao, J.; Uyanik, H.; Nadzir, Z.A.; Lou, Y. Evaluation of Sentinel-3A altimetry over Songhua river Basin. *J. Hydrol.* **2023**, *618*, 129197. [CrossRef]
124. Sheffield, J.; Wood, E.F.; Pan, M.; Beck, H.; Coccia, G.; Capdevila, A.S.; Verbist, K. Satellite Remote Sensing for Water Resources Management: Potential for Supporting Sustainable Development in Data-Poor Regions. *Water Resour. Res.* **2018**, *54*, 9724–9758. [CrossRef]
125. Li, J.Z.; Guo, X.L.; Gong, T.L.; Wang, J.; Wang, T.; Li, H. Monitoring and quantitative inversion of river flow in data-scarce areas without or with little data. *J. Hydraul. Eng.* **2018**, *49*, 9.
126. Mengen, D.; Ottinger, M.; Leinenkugel, P.; Ribbe, L. Modeling River Discharge Using Automated River Width Measurements Derived from Sentinel-1 Time Series. *Remote Sens.* **2020**, *12*, 3236. [CrossRef]
127. Gleason, C.J.; Durand, M.T. Remote Sensing of River Discharge: A Review and a Framing for the Discipline. *Remote Sens.* **2020**, *12*, 1107. [CrossRef]
128. Jiang, L.P.; Ding, J.L.; Bao, Q.L.; Ge, X.Y.; Liu, J.M.; Wang, J.J. Inversion of river flow based on low-altitude remote sensing combined with satellite images—Taking the Kashgar River as an example. *Arid. Land Geogr.* **2023**, *46*, 385–396.

129. Ma, J.; Lu, S.L.; Qi, J.G.; Zhai, Z.K. Study on remote sensing estimation model of river flow in hydrological data scarce area. *Sci. Surv. Mapp.* **2019**, *44*, 184–190.
130. Chen, Q.X.; Zhang, Y.P.; Li, J.D. Estimation of river flow based on SPOT5 remote sensing image and DEM. *People's Pearl River* **2019**, *40*, 39–45.
131. Lin, P.; Pan, M.; Beck, H.E.; Yang, Y.; Dai, Y.; Frasson, R.; David, C.H.; Durand, M.; Pavelsky, T.M.; Allen, G.H. Global Reconstruction of Naturalized River Flows at 2.94 Million Reaches. *Water Resour. Res.* **2019**, *55*, 6499–6516. [CrossRef]
132. Lu, S.L.; Wu, B.F.; Yan, N.N. Research progress on remote sensing monitoring of river runoff. *Adv. Earth Sci.* **2010**, *25*, 7.
133. Li, H.M.; Bai, J.; Gan, F.P.; Li, X.Q.; Wang, Z.K. Research progress on remote sensing estimation of river flow. *Nat. Resour. Remote Sens.* **2018**, *10*, 1385.
134. Yang, G. *Research on River Flow Measurement Based on CNN and Image Processing*; Shandong University: Jinan, China, 2021.
135. Wu, F.A.; Chen, Y.; Yang, S.T. Changes in glacial meltwater runoff and its response to climate change in the Tianshan region detected using unmanned aerial vehicles (UAVs) and satellite remote sensing. *Water* **2021**, *13*, 1753.
136. Zhang, Z.; Zhou, Y.; Guo, H.L.; Zhou, L.; Li, N.G.; Fu, W.J.; Gao, W.J.; Zhu, J.B. Application of Video Flow Measurement System in High Flood Monitoring. In Proceedings of the Third Volume of the 2019 Annual Conference of the China Water Conservancy Society, Yichang, China, 25 October 2019; pp. 437–446.
137. Zhao, C.S.; Pan, X.; Yang, S.T.; Liu, C.M.; Chen, X.; Zhang, H.M.; Pan, T.L. Inversion of River Flow Based on Low-altitude Remote Sensing Unmanned Aerial Vehicle Images. *Acta Geogr. Sin.* **2019**, *74*, 1392–1408.
138. Tarpanelli, A.; Brocca, L.; Lacava, T.; Melone, F.; Moramarco, T.; Faruolo, M.; Pergola, N.; Tramutoli, V. Toward the estimation of river discharge variations using MODIS data in ungauged basins. *Remote Sens. Environ.* **2013**, *136*, 47–55. [CrossRef]
139. Sichangi, A.W.; Wang, L.; Yang, K.; Chen, D.; Wang, Z.; Li, X.; Zhou, J.; Liu, W.; Kuria, D. Estimating continental river basin discharges using multiple remote sensing data sets. *Remote Sens. Environ.* **2016**, *179*, 36–53. [CrossRef]
140. Lei, Z.D.; Hu, H.P.; Yang, S.X. Advances and Review of Soil Water Research. *Adv. Water Sci.* **1999**, *10*, 311–318.
141. Shi, J.C.; Du, Y.; Du, J.Y.; Jiang, L.M.; Chai, L.N.; Mao, K.B.; Xu, P.; Ni, W.J.; Xiong, C.; Liu, Q.; et al. Progress in Microwave Remote Sensing Surface Parameter Inversion. *Sci. China Earth Sci.* **2012**, *42*, 814–842.
142. Wigneron, J.P.; Waldteufel, P.; Chanzy, A.; Calvet, J.C.; Kerr, Y. Two-Dimensional Microwave Interferometer Retrieval Capabilities over Land Surfaces (SMOS Mission). *Remote Sens. Environ.* **2017**, *73*, 270–282. [CrossRef]
143. Wu, Z.M.; Qiu, J.X.; Liu, S.X.; Mo, X.G. Research Progress on Agricultural Drought Monitoring Based on Soil Moisture. *Prog. Geogr.* **2020**, *39*, 1758–1769. [CrossRef]
144. Li, Z.J.; Chen, J.P.; Liu, Y.M.; Yao, X.L.; Yu, J.S. Research Progress in Remote Sensing Inversion of Soil Moisture. *J. Beijing Norm. Univ. (Nat. Sci.)* **2020**, *56*, 474–481.
145. Dorigo, W.A.; Xaver, A.; Vreugdenhil, M. Global Automated Quality Control of In Situ Soil Moisture Data from the International Soil Moisture Network. *Vadose Zone J.* **2013**, *12*, 918–924. [CrossRef]
146. Rui, X.F. Discussion on Watershed Hydrological Model. *Adv. Sci. Technol. Water Resour.* **2017**, *37*, 1–7.
147. Liang, X.; Lettenmaier, D.P.; Wood, E.F.; Burges, S.J. A simple hydrologically based model of land surface water and energy fluxes for general circulation models. *J. Geophys. Res. Atmos.* **1994**, *99*, 14415–14428. [CrossRef]
148. Wu, X.; Lu, G.; Wu, Z.; He, H.; Dorigo, W. Triple Collocation-Based Assessment of Satellite Soil Moisture Products with in situ Measurements in China: Understanding the Error Sources. *Remote Sens.* **2020**, *12*, 2275. [CrossRef]
149. Chen, S.L.; Liu, Y.B.; Wen, Z.M. Review on Satellite Remote Sensing Inversion of Soil Moisture. *Adv. Earth Sci.* **2012**, *27*, 1192–1203.
150. Kong, J.L.; Li, J.J.; Zhen, P.P.; Yang, X.T.; Yang, J.; Wu, Z.C. Study on Synergetic Inversion of Soil Moisture in Arid Area Based on Microwave and Optical Remote Sensing. *J. Geo-Inf. Sci.* **2016**, *18*, 857–863.
151. Chen, F.; Crow, W.T.; Colliander, A.; Cosh, M.H.; Jackson, T.J.; Bindlish, R.; Reichle, R.H.; Chan, S.K.; Bosch, D.D.; Starks, P.J. Application of Triple Collocation in Ground-Based Validation of Soil Moisture Active/Passive (SMAP) Level 2 Data Products. *IEEE J. Sel. Top. Appl. Earth Obs. Remote Sens.* **2017**, *10*, 489–502. [CrossRef]
152. Gruber, A.; Scanlon, T.; Schalie, R.; Wagner, W.; Dorigo, W. Evolution of the ESA CCI Soil Moisture climate data records and their underlying merging methodology. *Earth Syst. Sci. Data* **2019**, *11*, 717–739. [CrossRef]
153. Wagner, W.; Hahn, S.; Kidd, R.; Melzer, T.; Bartalis, Z.; Hasenauer, S.; Figa-Saldaña, J.; De Rosnay, P.; Jann, A.; Schneider, S. The ASCAT Soil Moisture Product: A Review of its Specifications, Validation Results, and Emerging Applications. *Meteorol. Z* **2013**, *22*, 5–33. [CrossRef]
154. Al-Yaari, A.; Wigneron, J.P.; Dorigo, W.; Colliander, A.; Pellarin, T.; Hahn, S.; Mialon, A.; Richaume, P.; Fernandez-Moran, R.; Fan, L. Assessment and inter-comparison of recently developed/reprocessed microwave satellite soil moisture products using ISMN ground-based measurements. *Remote Sens. Environ.* **2019**, *224*, 289–303. [CrossRef]
155. Crow, W.T.; Berg, A.A.; Cosh, M.H.; Loew, A.; Mohanty, B.P.; Panciera, R.; Rosnay, P.D.; Ryu, D.; Walker, J.P. Upscaling sparse ground-based soil moisture observations for the validation of coarse-resolution satellite soil moisture products. *Rev. Geophys.* **2012**, *50*, 2. [CrossRef]
156. Zheng, Y.F.; Huang, T.N.; Duan, C.C.; Yin, J.F.; Wu, R.J. Research Progress on Microwave Remote Sensing Soil Moisture Inversion Algorithm and Product. *Jiangsu Agric. Sci.* **2017**, *45*, 1–7.
157. Kerr, Y.H.; Al-Yaari, A.; Rodriguez-Fernandez, N.; Parrens, M.; Molero, B.; Leroux, D.; Bircher, S.; Mahmoodi, A.; Mialon, A.; Richaume, P.; et al. Overview of SMOS performance in terms of global soil moisture monitoring after six years in operation. *Remote Sens. Environ.* **2016**, *180*, 40–63. [CrossRef]

158. Parrens, M.; Wigneron, J.P.; Richaume, P.; Mialon, A.; Bitar, A.A.; Fernandez-Moran, R.; Al-Yaari, A.; Kerr, Y.H. Global-scale surface roughness effects at L-band as estimated from SMOS observations. *Remote Sens. Environ.* **2016**, *181*, 122–136. [CrossRef]
159. Zhang, X.; Zhang, T.; Zhou, P.; Shao, Y.; Gao, S. Validation Analysis of SMAP and AMSR2 Soil Moisture Products over the United States Using Ground-Based Measurements. *Remote Sens.* **2017**, *9*, 104. [CrossRef]
160. Cho, E.; Su, C.H.; Ryu, D.; Kim, H.; Choi, M. Does AMSR2 produce better soil moisture retrievals than AMSR-E over Australia? *Remote Sens. Environ.* **2017**, *188*, 95–105. [CrossRef]
161. Chen, F.; Crow, W.T.; Bindlish, R.; Colliander, A.; Burgin, M.S.; Asanuma, J.; Aida, K. Global-scale evaluation of SMAP, SMOS and ASCAT soil moisture products using triple collocation. *Remote Sens. Environ.* **2018**, *214*, 1–13. [CrossRef]
162. Liu, Y.L.Y.; Yang, Y.Y.Y.; Yue, X.Y.X. Evaluation of Satellite-based Soil Moisture Products over Four Different Continental In-situ Measurements. *Remote Sens.* **2018**, *10*, 1161. [CrossRef]
163. González-Zamora, Á.A.A.U.; Sánchez, N.A.N.U.; Pablos, M.A.M.U.; Martínez-Fernández, J.A.J.U. CCI soil moisture assessment with SMOS soil moisture and in situ data under different environmental conditions and spatial scales in Spain. *Remote Sens. Environ.* **2019**, *225*, 469–482. [CrossRef]
164. Ma, H.A.; Zeng, J.A.; Chen, N.A.C.W.; Zhang, X.A.; Cosh, M.H.A.; Wang, W.A. Satellite surface soil moisture from SMAP, SMOS, AMSR2 and ESA CCI: A comprehensive assessment using global ground-based observations. *Remote Sens. Environ.* **2019**, *2019*, 111215. [CrossRef]
165. Deng, K.D.K.A.; Lamine, S.L.S.; Pavlides, A.P.A.; Petropoulos, G.P.G.P.; Srivastava, P.S.P.K.; Bao, Y.B.Y.; Hristopulos, D.H.D.; Anagnostopoulos, V.A.V. Operational Soil Moisture from ASCAT in Support of Water Resources Management. *Remote Sens.* **2019**, *11*, 579. [CrossRef]
166. Zhang, R.; Kim, S.; Sharma, A. A comprehensive validation of the SMAP Enhanced Level-3 Soil Moisture product using ground measurements over varied climates and landscapes. *Remote Sens. Environ.* **2019**, *223*, 82–94. [CrossRef]
167. Singh, A.; Gaurav, K.; Meena, G.K.; Kumar, S. Estimation of Soil Moisture Applying Modified Dubois Model to Sentinel-1; A Regional Study from Central India. *Remote Sens.* **2020**, *12*, 2266. [CrossRef]
168. Mohseni, F.; Mirmazloumi, S.M.; Mokhtarzade, M.; Jamali, S.; Homayouni, S. Global Evaluation of SMAP/Sentinel-1 Soil Moisture Products. *Remote Sens.* **2022**, *14*, 4624. [CrossRef]
169. Yu, W.; Li, Y.; Liu, G. Calibration of the ESA CCI-Combined Soil Moisture Products on the Qinghai-Tibet Plateau. *Remote Sens.* **2023**, *15*, 918. [CrossRef]
170. Paloscia, S.; Pettinato, S.; Santi, E.; Notarnicola, C.; Pasolli, L.; Reppucci, A. Soil moisture mapping using Sentinel-1 images: Algorithm and preliminary validation. *Remote Sens. Environ.* **2013**, *134*, 234–248. [CrossRef]
171. Su, Z.; Wen, J.; Dente, L.; Van, D.V.R.; Wang, L.; Ma, Y.; Yang, K.; Hu, Z. The Tibetan Plateau observatory of plateau scale soil moisture and soil temperature (Tibet-Obs) for quantifying uncertainties in coarse resolution satellite and model products. *Hydrol. Earth Syst. Sci.* **2017**, *15*, 2303. [CrossRef]
172. Yao, P.P. *Spatiotemporal Extension Research on Microwave Remote Sensing Soil Moisture*; Institute of Remote Sensing and Digital Earth (Chinese Academy of Sciences): Beijing, China, 2018.
173. Lan, X.Y.; Guo, Z.Q.; Tian, Y.; Lei, X.; Wang, J. Review on assimilation research of remote sensing estimation of soil moisture. *Adv. Earth Sci.* **2015**, *30*, 668–679.
174. Liang, S.L.; Bai, R.; Chen, X.N.; Cheng, J.; Fan, W.J.; He, T.; Jia, K.; Jiang, B.; Jiang, L.M.; Jiao, Z.T. Development review on quantitative remote sensing for land surface in China in 2019. *J. Remote Sens.* **2020**, *24*, 54.
175. Ma, M.G.; Wang, J.; Wang, X.M. Advances in research on interannual variation of vegetation based on remote sensing. *J. Remote Sens.* **2006**, *10*, 421–431.
176. Fensholt, R.; Langanke, T.; Rasmussen, K.; Reenberg, A.; Prince, S.D.; Tucker, C.; Scholes, R.J.; Le, Q.B.; Bondeau, A.; Eastman, R. Greenness in semi-arid areas across the globe 1981–2007—An Earth Observing Satellite based analysis of trends and drivers. *Remote Sens. Environ.* **2012**, *121*, 144–158. [CrossRef]
177. Du, Z.M.; Ma, W.M.; Zhou, Q.P.; Chen, H.; Deng, Z.Z.M.; Liu, J.Q. Research progress of vegetation identification method based on remote sensing technology. *Ecol. Sci.* **2022**, *41*, 222–229.
178. Wang, Z.; Zhao, L.J.; Niu, K.; Zhang, Y.; Yang, H. Research review of vegetation coverage extraction method based on remote sensing images. *Agric. Technol.* **2021**, *41*, 5.
179. Rao, K.; Anderegg, W.; Sala, A.; Martínez-Vilalta, J.; Konings, A.G. Satellite-based vegetation optical depth as an indicator of drought-driven tree mortality. *Remote Sens. Environ.* **2019**, *227*, 125–136. [CrossRef]
180. Yan, G.; Hu, R.; Luo, J.; Weiss, M.; Jiang, H.; Mu, X.; Xie, D.; Zhang, W. Review of indirect optical measurements of leaf area index: Recent advances, challenges, and perspectives. *Agric. Forest Meteorol.* **2019**, *265*, 390–411. [CrossRef]
181. Zhao, Y.H.; Hou, P.; Jiang, J.M.; Jiang, Y.; Zhang, B.; Bai, J.J.; Xu, H.T. Research progress of quantitative inversion method for vegetation ecological remote sensing parameters. *J. Remote Sens.* **2021**, *25*, 2173–2197.
182. Liu, Z.; Wan, W.; Huang, J.Y.; Han, Y.W.; Wang, J.Y. Research progress in key parameter inversion of crop growth based on unmanned aerial vehicle remote sensing. *Trans. Chin. Soc. Agric. Eng.* **2018**, *34*, 12.
183. Yue, J.; Yang, G.; Tian, Q.; Feng, H.; Xu, K.; Zhou, C. Estimate of winter-wheat above-ground biomass based on UAV ultrahigh-ground-resolution image textures and vegetation indices. *ISPRS J. Photogramm.* **2019**, *150*, 226–244. [CrossRef]
184. Hr, A.; Ml, A.; Jha, B. Estimating fractional cover of tundra vegetation at multiple scales using unmanned aerial systems and optical satellite data. *Remote Sens. Environ.* **2019**, *224*, 119–132.

185. Cao, Z.S.; Li, Y.D.; Huang, J.B.; Ye, C.; Sun, B.F.; Shu, S.F.; Zhu, Y.; He, Y. Monitoring rice leaf area index based on digital images from unmanned aerial vehicles. *Chin. J. Rice Sci.* **2022**, *36*, 308–317.
186. Chen, P.N.; Wang, R.Y.; Liu, H.Y.; Wang, L.; Yan, X.J.; Yin, T. Estimation of wheat field vegetation coverage based on satellite-unmanned aerial vehicle remote sensing data. *J. Henan Inst. Sci. Technol. (Nat. Sci. Ed.)* **2022**, *50*, 84.